Available online at www.sciencedirect.com
SCIENCE DIRECT
ELSEVIER
European Journal of Mechanics B/Fluids 25 (2006) 435–458
EUROPEAN JOURNAL OF MECHANICS B/FLUIDS

Dynamics of superfluid ^{4}He: Two-scale approach

Tomasz Lipniacki

Institute of Fundamental Technological Research, Department of Physics and Mechanics of Fluids, Swietokrzyska 21, 00-049 Warsaw, Poland

Received 29 September 2005; received in revised form 20 March 2006; accepted 10 April 2006

Abstract

The paper explores the two scale approach to the incompressible dynamics of superfluid ^{4}He. The fluid is described by a system of equations: Navier–Stokes and Euler equations for the macroscopic normal and superfluid velocity fields respectively. The two equations couple via a mutual friction force exerted on superfluid (quantum) vortices by the normal component. The magnitude of this force, calculated via the analysis of dynamics of quantum vortices in the microscopic scale, is proportional to the value of the counterflow (relative velocity of two helium components) and to the density of quantum vortices. The latter is determined by the generalized Vinen equation, adequate for flows having a net macroscopic vorticity. The generalized equation includes the drift of the anisotropic vortex tangle caused by Magnus force. The derived system of equations is applied first to the analysis of steady state solution of rotating turbulence, and then to the numerical analysis of formation of plane Couette flow between two infinite parallel material surfaces $z = 0$ and $z = D$. For $t < 0$ both surfaces and the fluid are at rest, then at $t = 0$ one material surface starts moving along the x axis with velocity V_0. The viscosity forces cause the motion of normal component and the counterflow which make the line-length density grow, and the two components become coupled by the mutual friction. The fact that superfluid velocity tends to match with the normal velocity makes that $\boldsymbol{\omega}_s \neq 0$, which implies polarization and drift of the tangle. At a given temperature the dynamics depends solely on DV_0.

Keywords: Dynamics of ^{4}He; Quantum turbulence; Anisotropy of quantum tangle; Rotating turbulence

1. Introduction

According to the Landau two-fluid model superfluid He II may be regarded as mixture of normal fluid and superfluid, described by the velocity fields $\mathbf{V}_s$ and $\mathbf{V}_n$ and the density fields ρ_n and ρ_s, respectively, where $\rho = \rho_s + \rho_n$ is the total density of He II. The densities ρ_s and ρ_n can be measured in a variety of ways and are known quite accurately as a function of pressure p and temperature T; if $T \to 0$ then $\rho_n \to 0$ and He II becomes a pure superfluid; if $T \to T_\lambda$, the temperature of the λ transition, then $\rho_s \to 0$ and He II becomes He I, which is a classical fluid. The rotationless flow of superfluid component is violated on one dimensional singularities called quantum or superfluid vortices. Due to the existence of such singularities, the superfluid component is coupled dissipatively to the normal one by the so-called mutual friction force $\mathbf{F}_{ns}$, which is proportional to the density of superfluid vortices L, and to the magnitude of counterflow $\mathbf{V}_{ns} = \mathbf{V}_n - \mathbf{V}_s$. At very low velocities it is expected, that the flows of normal and superfluid components are laminar and the quantum vortices form an ordered array of locally parallel lines. At higher velocities

E-mail address: tlipnia@ippt.gov.pl (T. Lipniacki).

0997-7546/$ – see front matter
doi:10.1016/j.euromechflu.2006.04.004

the superfluid laminar flow develops into a superfluid turbulent flow in which quantum vortices form a chaotic tangle. The simplest way to generate the tangle of quantum vortices is to seal one end of the channel and place a resistor there. According to the two-fluid model the normal fluid carries the heat away from the resistor being replaced by a superfluid, which must flow towards the heater to maintain a zero mass flux $\rho_s \mathbf{V}_s + \rho_n \mathbf{V}_n = 0$. In this way an internal counterflow $\mathbf{V}_{ns}$ whose magnitude is proportional to magnitude of heat flux $\dot{Q}$ is set up. If the heat flux (and so the counterflow) exceeds some critical value, the remnant vortices stretch and develop into the quantum tangle, which breaks the perfect heat conducting property.

The successive works by Vinen, Tough, Donnelly, Niemirowski and Fiszdon, among others, together with numerical simulations of Schwarz have clarified the nature of the counterflow tangle (see [1–3] for review). Important questions remain, however, concerning the turbulence in helium II produced by other techniques: Couette flow [4], rotating propellers [5] and towed grids [6]. The recent interest in helium turbulence is motivated by the study of high Reynolds number isothermal flows and the construction of a superfluid wind tunnel [7]. These flows, like heat currents, may induce intense vortex tangles with very a large vortex line density L. The measurements suggest that at high Reynolds number the vortices of the superfluid $\boldsymbol{\omega}_s$ and of the normal fluid $\boldsymbol{\omega}_n$ match dynamically over many length scales. This result adds to the evidence that the mechanically generated superfluid turbulence is similar to the classical turbulence, which can be explained by the observation that the high density of quantized vortex lines, present in the superfluid, locks together the normal fluid and the superfluid via mutual friction. One should expect that in the case when the macroscopic superfluid vorticity $\boldsymbol{\omega}_s$ matches over a certain length scale with the normal fluid vorticity field $\boldsymbol{\omega}_n$, the tangle of quantized vortices is highly anisotropic. This is in contrast to the quasi-isotropic turbulence generated in the counterflow channel described by (Schwarz)–Vinen [8] equation for line-length density L. In his pioneering works on microscopic dynamics of quantum tangle Schwarz [9,8] showed that quantized vortex lines can be approximated by classical vortex filaments of infinitesimal thickness whose motion is governed by the curvature. Schwarz showed that the vortex lines form a self-sustaining tangle driven by the counterflow $\mathbf{V}_{ns}$, which he assumed to be constant and uniform. He based his numerical investigations of tangle dynamics on the localized induction approximation [12] (LIA), which retains only the effects of local curvature, and on the assumption that lines reconnect when they cross. However, in the case when tangle carries the net macroscopic vorticity, the assumption that superfluid and normal fluid velocity fields are uniform is not longer justified and cannot be applied. On the other hand, when the superflow at high Reynolds numbers is considered, one may not expect that the superfluid vortex lines form an array of parallel lines, which will allow one to use the Hall–Vinen–Bekarevich–Khalatnikov [13] (HBVK) equations, adequate only for very low velocity flows. This difficulty has, been to a certain extent, overcome in the numerical simulations by Tsubota et al. [14–16] and the group of Barenghi and Samuels [17–19] and Kondaurova with Niemirowskii [20] in which the dynamics of the whole tangle was analyzed with help of the Biot–Savart law.

2. The model

2.1. Governing assumptions

In this paper we explore the two scale approach to the superfluid dynamics. In the macroscopic scale we use the two-fluid model equations; the Euler equation for the superfluid component and the Navier–Stokes equation for the normal component. The two equations are coupled by the mutual friction force, which depends on the local line-length density L. The density L at a given point, say P, is calculated in a small volume Ω around P, based on the Vinen equation, which is modified to describe the evolution of line-length density of the quantum tangle with net macroscopic vorticity. The generalized equation includes the drift of the anisotropic tangle caused by the Magnus force. The volume Ω, must be large enough to contain a large number of vortex lines, but small when compared with the integral scale of the flow. It is assumed that the normal and the superfluid velocity fields $\mathbf{V}_n$ and $\mathbf{V}_s$, given in the macroscopic scale by the Euler and the Navier-Stokes equations, respectively, are constant in the microscopic scale, across the volume Ω. The last assumption restricts our considerations to the case in which the normal flow is laminar, see [11] for discussion of this regime. Using the Vinen equation implies, in fact, that we base our approach on LIA, but only in the smallest length scale.

There are also two time scales considered in the problem; fast, connected with the local relaxation of the quantum vortex tangle and slow, connected with the evolution of the macroscopic variables: the normal and the superfluid velocity fields $\mathbf{V}_n$ and $\mathbf{V}_s$ and the line-length density L. The local relaxation of the tangle is due mostly to reconnections,

which cause, as shown by Schwarz [10], all the local derivatives of the vortex line to randomize. The characteristic randomization time is of the order of $T_R = \delta/v_l$, where δ is the typical interline spacing and v_l is the average self-induced velocity. The fact that the local derivatives of the vortex line randomize, does not imply that they average to zero when calculated over the volume Ω. As we will show the average binormal must be non-zero in the steady-state counterflow turbulence, and the average tangent is proportional to $\mathrm{rot}\mathbf{V}_s/L$. We will assume as in [21] that the randomization is manifested by such a configuration of the vortex lines which has the most probable distribution of the tangent (or binormal) given the prescribed mean.

We will thus assume, following Schwarz [8], that the geometric measures of the tangle defined in Section 2.3 are constant or they adjust themselves immediately to the slowly varying macroscopic variables $\mathbf{V}_n$, $\mathbf{V}_s$ and L. This assumption exclude the analysis of the very rapid transients, when counterflow direction or magnitude changes abruptly, since in this case, as shown in [21], the average binormal depart substantially from its steady-state value.

The proposed approach is, to some extent, similar to the non-local approximation (NLA); the numerical method proposed by Barenghi et al. [22] to calculate the growth of the quantum tangle in imposed ABC flow of normal flow. According to NLA the motion of vortex filaments is calculated using LIA, but in the superfluid velocity field which is calculated in a relatively small number of points, based on the Biot–Savart law. This numerical method captures non-local interaction, but is much faster than the direct method, in which the Biot–Savart law is applied to calculate superfluid velocity on every vortex line. An analogous idea is present in the work by Idowu et al. [23], however the authors assume that the mutual friction is proportional to macroscopic superfluid vorticity $\boldsymbol{\omega}_s$, which is justified only when the vortices form a locally parallel system of lines. In reality, even when $\boldsymbol{\omega}_s$ is small, the mutual friction can be significant due to the dense tangle of quantum vortices. It is also hard to imagine how line length (and so the vorticity of superfluid) may be effectively generated in the volume, if the vortex lines remain locally parallel.

2.2. Incompressible two-fluid equations

The two fluid model is described by the equations of motion which can be written as (Donnelly [24])

$$\rho_s\left(\frac{\partial \mathbf{V}_s}{\partial t} + \mathbf{V}_s\cdot\nabla\mathbf{V}_s\right) = -\frac{\rho_s}{\rho}\nabla p + \rho_s S\nabla T - \mathbf{F}_{ns}, \tag{1}$$

$$\rho_n\left(\frac{\partial \mathbf{V}_n}{\partial t} + \mathbf{V}_n\cdot\nabla\mathbf{V}_n\right) = -\frac{\rho_n}{\rho}\nabla p - \rho_s S\nabla T + \mathbf{F}_{ns} + \eta\Delta^2\mathbf{V}_n. \tag{2}$$

Eq. (1) is the Euler equation for the superfluid, (2) the Navier–Stokes equation for the normal component having the viscosity η. These two equations are coupled by the mutual friction $\mathbf{F}_{ns}$. The terms $\rho_s S\nabla T$ represent fountain pressure. The terms $\frac{\rho_n\rho_s}{2\rho}\nabla(\mathbf{V}_{ns})^2$, present in some formulations (e.g. Donnelly [1]), are neglected here.

In this paper we confine ourselves to the so-called incompressible approximation: $\rho_s = \text{const}$, $\rho_n = \text{const}$. The resulting equations read

$$\mathrm{div}\,\mathbf{V}_n = \mathrm{div}\,\mathbf{V}_s = 0, \tag{3}$$

$$\rho_s\left(\frac{\partial \mathbf{V}_s}{\partial t} + \mathbf{V}_s\cdot\nabla\mathbf{V}_s\right) = -\nabla p_s - \mathbf{F}_{ns}, \tag{4}$$

$$\rho_n\left(\frac{\partial \mathbf{V}_n}{\partial t} + \mathbf{V}_n\cdot\nabla\mathbf{V}_n\right) = -\nabla p_n + \mathbf{F}_{ns} + \eta\Delta^2\mathbf{V}_n, \tag{5}$$

where p_s, p_n are the effective pressures,

$$\nabla p_s = \frac{\rho_s}{\rho}\nabla P - \rho_s S\nabla T, \tag{6}$$

$$\nabla p_n = \frac{\rho_n}{\rho}\nabla P + \rho_s S\nabla T. \tag{7}$$

To close the system of Eqs. (3)–(5) we have to determine the mutual friction force $\mathbf{F}_{ns}$. In order to do this we have to refer to the microscopic vortex dynamics.

2.3. Modified Vinen equation

Let us recall: If a curve traced out by a vortex filament is specified in a parametric form, $\mathbf{s}(\xi, t)$, an instantaneous velocity of a given point of the filament in LIA reads

$$\dot{\mathbf{s}} = \mathbf{V}_s + \beta \mathbf{s}' \times \mathbf{s}'' + \alpha\beta \mathbf{s}'' + \alpha \mathbf{s}' \times \mathbf{V}_{ns}, \tag{8}$$

where the dot and the prime denote instantaneous derivatives with respect to time t and arc length ξ, respectively, while α is a dimensionless friction coefficient, and

$$\beta = \frac{\kappa}{4\pi} \ln\left(\frac{c}{a_o \langle|\mathbf{s}''|\rangle}\right) \approx \kappa, \tag{9}$$

where κ is the quantum of circulation, c is a constant of the order of 1, $\langle|s''|\rangle$ is the average curvature of vortices in the tangle and $a_o \simeq 1.3 \times 10^{-8}$ cm is the effective core radius of a quantized vortex. The second friction coefficient α' is small and, following Schwarz [8], all terms proportional to α' are neglected in Eq. (8).

If the motion of a vortex filament fulfills Eq. (8) and $\mathbf{V}_s$ is constant across the small volume Ω containing the filament, its line-length $l = \int \mathrm{d}\xi$ satisfies the following equation [8]:

$$\frac{\partial l}{\partial t} = \int \left(\alpha\, \mathbf{V}_{ns} \cdot (\mathbf{s}' \times \mathbf{s}'') - \alpha\beta |\mathbf{s}''|^2\right) \mathrm{d}\xi. \tag{10}$$

The first term of the r.h.s. of the above equation describes the dependence of the line-length on counterflow velocity. This term can be positive or negative, depending on the angle formed by the binormal to the vortex line ($\mathbf{b} = \mathbf{s}' \times \mathbf{s}''$), and the counterflow. It is straightforward that this term vanishes for a totally isotropic vortex tangle. Thus, in a steady state ($\mathrm{d}L/\mathrm{d}t = 0$), the vortex tangle cannot be totally isotropic since some directional anisotropy of the binormal is needed to balance the second term which is always negative.

To rewrite Eq. (10) in the form of Vinen equation we make use of the following characteristic measures of vortex tangle [8,21]. The line-length density is then

$$L = \frac{1}{\Omega} \int \mathrm{d}\xi. \tag{11}$$

Next we have

$$c_1 = \frac{1}{\Omega L^{3/2}} \int |\mathbf{s}''| \, \mathrm{d}\xi, \tag{12}$$

$$c_2^2 = \frac{1}{\Omega L^2} \int |\mathbf{s}''|^2 \, \mathrm{d}\xi, \tag{13}$$

$$\mathbf{I}_l = \frac{1}{\Omega L^{3/2}} \int \mathbf{s}' \times \mathbf{s}'' \, \mathrm{d}\xi, \tag{14}$$

$$\mathbf{I} = \mathbf{I}_l / c_1 = \frac{\langle \mathbf{s}' \times \mathbf{s}'' \rangle}{\langle |\mathbf{s}''| \rangle}. \tag{15}$$

The coefficients c_1 and c_2^2 measure the average curvature and average curvature squared of the tangle (in a sample volume Ω), while $\mathbf{I}$ is a vector that measures the anisotropy of the binormal to the vortex lines. For example, $\mathbf{I} = 0$ for an isotropic tangle and $I := |\mathbf{I}| = 1$ if all binormals to the vortex lines forming the tangle are parallel. The parameter I_l introduced by Schwarz is defined as $I_l = \widehat{\mathbf{V}}_{ns} \cdot \mathbf{I}_l$, where $\widehat{\mathbf{V}}_{ns} = \mathbf{V}_{ns}/|\mathbf{V}_{ns}|$ is the counterflow unit vector.

It should be noted that the description of the tangle via the characteristic measures defined above makes sense only if the volume Ω is large enough to contain many vortex lines. Using the above measures one can rewrite Eq. (10) in the following form:

$$\frac{\mathrm{d}L}{\mathrm{d}t} = \alpha\, L^{3/2} c_1 \mathbf{I} \cdot \mathbf{V}_{ns} - \beta\alpha {c_2}^2\, L^2. \tag{16}$$

The above equation is the Vinen equation with coefficients expressed as a function of the microscopic measures of the tangle. Schwarz [8] showed using the scaling arguments that for the equilibrium turbulence, the measures c_1, c_2 and I_l depend on neither L nor $\mathbf{V}_{ns}$, and evaluated them numerically for various friction parameters α for a homogeneous

vortex tangle. To analyze the transients he assumed that c_1, c_2, I_0 are constant, $\mathbf{I} = I_0\widehat{\mathbf{V}}_{ns}$, also when L departs from its equilibrium value. This assumption is crude, but was shown to be satisfactory [25] for relatively small transients. For large transients, or in the case, when counterflow direction changes abruptly, it was shown in [21] that Eq. (16) must be supplemented by at least one additional equation for anisotropy vector $\mathbf{I}$. Here, however, we follow the Schwarz assumption (neglecting the dependence of coefficients c_1, c_2, I_o on the $\mathbf{V}_{ns}$ and L) to concentrate on the modification that has to be made in the case when the tangle carries net macroscopic vorticity. Let us define

$$\boldsymbol{\omega}_s = \frac{\kappa}{\Omega}\int \mathbf{s}'\,\mathrm{d}\xi, \tag{17}$$

$$\mathbf{q} = \frac{\boldsymbol{\omega}_s}{\kappa L} = \frac{\int \mathbf{s}'\,\mathrm{d}\xi}{\int \mathrm{d}\xi}, \tag{18}$$

where $\boldsymbol{\omega}_s$ is interpreted as macroscopic superfluid vorticity i.e. $\boldsymbol{\omega}_s = \mathrm{rot}\,\mathbf{V}_s$. Vector $\mathbf{q}$, $|\mathbf{q}| = q \in [0,1]$ measures directional anisotropy of the tangent; $\mathbf{q} = 0$ for totally isotropic tangle and $|\mathbf{q}| = 1$ for a system of parallel vortices. We will assume that directional anisotropy $\mathbf{q}$ modifies curvature coefficients, but not the second anisotropy coefficient I_0; hence we replace $c_1,\ c_2$ by $\bar{c}_1(q),\ \bar{c}_2(q)$ in Eq. (16). It is obvious that $\bar{c}_1(0) = c_1,\ \bar{c}_2(0) = c_2$, and we expect also that both $\bar{c}_1(q),\ \bar{c}_2(q)$ decrease with q as lines forming the tangle become directionally oriented, in particular if $q \to 1$ then $\bar{c}_1 \to 0$, $\bar{c}_2 \to 0$.

For quantitative analysis we propose to replace $c_1,\ c_2$ by $\bar{c}_1(q),\ \bar{c}_2(q)$, where

$$\bar{c}_1(q) = c_1\big(1-q^2\big), \qquad \bar{c}_2(q) = c_2\big(1-q^2\big). \tag{19}$$

We assume that coefficients $c_1,\ c_2,\ I_0$ are constant and take them from Schwarz simulations of the steady-state tangle with no net superfluid vorticity [8]. The above choice of $\bar{c}_1(q),\ \bar{c}_2(q)$ will be justified in Appendix A.

To calculate the partial time derivative of L one has to take into account the drift of the tangle,

$$\frac{\partial L}{\partial t} = \alpha I_0 c_1\big(1-q^2\big)|\mathbf{V}_{ns}|L^{3/2} - \beta\alpha {c_2}^2\big(1-q^2\big)^2 L^2 - \mathrm{div}(L\mathbf{V}_L), \tag{20}$$

where $\mathbf{V}_L$ is the tangle drift velocity. The drift term is especially important for $q \neq 0$, since the tangle carrying net vorticity has the tendency to move across the flow. The drift velocity may be calculated by averaging the local vortex velocity over a sample volume Ω

$$\mathbf{V}_L = \frac{1}{\Omega L}\int \dot{\mathbf{s}}\,\mathrm{d}\xi. \tag{21}$$

Defining

$$\mathbf{I}_k = \frac{1}{\Omega L^{3/2}}\int \mathbf{s}''\,\mathrm{d}\xi, \tag{22}$$

and using Eq. (8) for $\dot{\mathbf{s}}$, we obtain $\mathbf{V}_L$ in the following form

$$\mathbf{V}_L = \mathbf{V}_s + \alpha\mathbf{q}\times\mathbf{V}_{ns} + \beta\alpha I_0 c_1\big(1-q^2\big)L^{1/2}\widehat{\mathbf{V}}_{ns} + \beta\alpha\mathbf{I}_k L^{1/2}. \tag{23}$$

The vector $\mathbf{I}_k$ represents the curvature of $\boldsymbol{\omega}_s$ lines and except for the case when the "tangle" consists of bent, but locally parallel, lines its magnitude is relatively small. It is precisely zero if the vortex lines are closed, isotropic or straight. We expect that in most situations the last term in the above equation can be neglected and to simplify the analysis we will not take it to the account.

2.4. An alternative derivation of the Vinen-type equation

The derivation of the generalized Vinen equation presented in the previous subsection bases on the idea introduced by Schwarz that both generation and decay of the vortex tangle are related to mutual friction. There is however another view, pioneered by Feyman who hypothesized that the decay of the vortex tangle results from the cascade-like breakdown of vortices due to the reconnections. In fact the Feyman idea can also lead us to the Vinen-type equation. In [26] (see also [27] for related analytical results) we showed that line-length change ΔL of two vortex lines resulting from the reconnection (in the presence of counterflow $\mathbf{V}_{ns}$) can be approximated in the form

$$\Delta L(a,b,t) = -a\beta^{1/2}\alpha^{1/2}t^{1/2} + b\beta^{-1/2}\alpha^{3/2}\mathbf{V}_{ns}^2 t^{3/2}, \tag{24}$$

where $a > 0, b \geqslant 0$ are nondimensional coefficients depending only on the geometric configuration of the reconnecting lines with respect to the counterflow, and t is time after the reconnection. One can estimate numerically the average coefficients $\bar{a}(q)$ and $\bar{b}(q)$ considering various reconnection configurations representative for the tangle of a given anisotropy q. In [28] we estimate the reconnection frequency f_r (number of reconnections per time per unit volume) as

$$f_r = c(q) v_l L^2, \tag{25}$$

where $v_l \simeq \beta L^{1/2}$ is the characteristic velocity of vortex lines in the tangle, and $c(q)$ is the nondimensional coefficient, such that $c(0) \simeq 1/2$. Finally, we may estimate the characteristic time between reconnections, t_0, i.e. the average time for which a vortex segment of length $L^{-1/2}$ can move without crossing the other vortex filament (which is roughly equal to the tangle randomization time T_R introduced by Schwarz [10], see Section 5)

$$t_0 = 1/c(q)\beta L. \tag{26}$$

Now, the time derivative of the line-length density reads [28]

$$\frac{\mathrm{d}L}{\mathrm{d}t} = f_r \times \Delta L\big(\bar{a}(q), \bar{b}(q), t_0\big) = c(q)^{-1/2}\bar{b}(q)\beta^{-1}\alpha^{3/2} L V_{ns} - c(q)^{1/2}\bar{a}(q)\beta\alpha^{1/2}L^2. \tag{27}$$

The above equation strictly corresponds to the so-called alternative Vinen equation [29], and in fact predicts the growth and decay profiles which are almost indistinguishable from these of the classical Vinen equation. We have estimated numerically the coefficients $\bar{a}(q)$ and $\bar{b}(q)$ for $q = 0$, i.e. assuming the directional isotropy of vortex lines: $\bar{a}(0) = 2.34$ and $\bar{b}(0) = 0.514$. From our derivation [28] we may expect that the reconnection frequency is a decreasing function of the anisotropy coefficient q. The analysis in [26] suggests also that coefficients $\bar{a}(q)$ and $\bar{b}(q)$ may substantially vary with q. Assuming, as done in Appendix A, that the distribution of the tangent is the most probable distribution which gives the prescribed $\mathbf{q}$ one can possibly estimate functions $c(q)$, $\bar{a}(q)$ and $\bar{b}(q)$ and thus generalize Eq. (27), on the anisotropic tangle. The advantage of the above derivation is that the numerical simulations needed to determine $\bar{a}(q)$ and $\bar{b}(q)$ are much simpler than these of Schwarz, since we need to simulate only the single vortex evolution in a number of sample configurations. The disadvantage is that it uses several uncertain assumptions, and this is why we based our current approach on the idea introduced by Schwarz.

2.5. Mutual friction

The normal fluid exerts on quantum vortices the so-called drag force $\mathbf{f}_D$,

$$\mathbf{f}_D = \alpha\rho_s\kappa\big(\mathbf{s}' \times (\mathbf{s}' \times \mathbf{V}_{ns}) + \beta\mathbf{s}' \times \mathbf{s}''\big). \tag{28}$$

This force averaged over a sample volume Ω gives the mutual friction force $\mathbf{F}_{ns}$, (in fact $\mathbf{F}_{ns}$ is the density of force)

$$\mathbf{F}_{ns} = \frac{1}{\Omega}\int \mathbf{f}_D \,\mathrm{d}\xi. \tag{29}$$

Defining vector $\mathbf{I}_v$,

$$\mathbf{I}_v = \frac{1}{\Omega L}\int \mathbf{s}'(\mathbf{s}' \cdot \mathbf{V}_{ns})\,\mathrm{d}\xi, \tag{30}$$

one can express $\mathbf{F}_{ns}$ in the following form

$$\mathbf{F}_{ns} = \alpha\kappa\rho_s L\big(\mathbf{I}_v - \mathbf{V}_{ns} + \beta I_0 c_1\big(1-q^2\big)L^{1/2}\widehat{\mathbf{V}}_{ns}\big). \tag{31}$$

Vector $\mathbf{I}_v$ depends on $\mathbf{q}$ and $\mathbf{V}_{ns}$ and, as we show in Appendix A, it can be approximated in the following form:

$$\mathbf{I}_v = \mathbf{q}(\mathbf{q} \cdot \mathbf{V}_{ns}) + \mathbf{V}_{ns}\left(\frac{1-q^2}{3}\right). \tag{32}$$

The above, together with Eq. (31), yields

$$\mathbf{F}_{ns} = \alpha\kappa\rho_s L\left(\mathbf{q} \times (\mathbf{q} \times \mathbf{V}_{ns}) - \frac{2}{3}\mathbf{V}_{ns}\big(1-q^2\big) + \beta I_0 c_1\big(1-q^2\big)L^{1/2}\widehat{\mathbf{V}}_{ns}\right). \tag{33}$$

3. The ^{4}He dynamics equations

3.1. The equations

The derived equations add up to the following closed system:

$$\operatorname{div}\mathbf{V}_n = \operatorname{div}\mathbf{V}_s = 0, \tag{34}$$

$$\rho_s\left(\frac{\partial \mathbf{V}_s}{\partial t} + \mathbf{V}_s\cdot\nabla\mathbf{V}_s\right) = -\nabla p_s - \mathbf{F}_{ns}, \tag{35}$$

$$\rho_n\left(\frac{\partial \mathbf{V}_n}{\partial t} + \mathbf{V}_n\cdot\nabla\mathbf{V}_n\right) = -\nabla p_n + \mathbf{F}_{ns} + \eta\Delta^2\mathbf{V}_n, \tag{36}$$

with

$$\mathbf{F}_{ns} = \alpha\kappa\rho_s L\left(\mathbf{q}\times\left(\mathbf{q}\times\mathbf{V}_{ns}\right) - \frac{2}{3}\mathbf{V}_{ns}\left(1-q^2\right) + \beta I_0 c_1\left(1-q^2\right)L^{1/2}\widehat{\mathbf{V}}_{ns}\right), \tag{37}$$

$$\frac{\partial L}{\partial t} = \alpha I_0 c_1\left(1-q^2\right)|\mathbf{V}_{ns}|L^{3/2} - \beta\alpha {c_2}^2\left(1-q^2\right)^2 L^2 - \operatorname{div}(L\mathbf{V}_L), \tag{38}$$

where

$$\mathbf{V}_L = \mathbf{V}_s + \alpha\mathbf{q}\times\mathbf{V}_{ns} + \beta\alpha I_0 c_1\left(1-q^2\right)L^{1/2}\widehat{\mathbf{V}}_{ns}, \tag{39}$$

$$\mathbf{V}_{ns} = \mathbf{V}_n - \mathbf{V}_s, \tag{40}$$

$$\mathbf{q} = \frac{\nabla\times\mathbf{V}_s}{\kappa L}, \qquad q = |\mathbf{q}|, \tag{41}$$

where $\rho_s,\ \rho_n,\ \eta,\ \alpha,\ \beta \approx \kappa,\ \kappa,\ c_1,\ c_2,\ I_0$, are temperature dependent constants. For the quantitative analysis the alternative expression for $\mathbf{F}_{ns}$ may be useful

$$\mathbf{F}_{ns} = \alpha\kappa\rho_s L\left(\mathbf{q}(\mathbf{q}\cdot\mathbf{V}_{ns}) - \mathbf{V}_{ns}\left(\frac{2+q^2}{3}\right) + \beta I_0 c_1\left(1-q^2\right)L^{1/2}\widehat{\mathbf{V}}_{ns}\right). \tag{42}$$

The macroscopic Euler and Navier–Stokes equations (35), (36) for normal and superfluid velocity fields, are coupled by the mutual friction force $\mathbf{F}_{ns}$, which is given by Eq. (37). The mutual friction depends on line-length density L, determined by Eq. (38). The system is closed by Eqs. (39)–(41) for the tangle drift velocity $\mathbf{V}_L$, counterflow $\mathbf{V}_{ns}$, and anisotropy vector $\mathbf{q}$.

The last terms in Eq. (42) (or (37)) and Eq. (39), respectively, result from the drift of the tangle in the direction of the counterflow, caused by its anisotropy $\mathbf{I} = I_o\widehat{\mathbf{V}}_{ns}$. It seems that in most cases these terms add nothing to the qualitative analysis of the system because they are relatively small and are directed along the counterflow [8].

The trivial solution of the system (34)–(41) is $\mathbf{V}_s = \mathbf{V}_n = L = 0$. However, even if macroscopic velocities of super and normal fluid are kept zero for a very long time, experiments show that there remains some non-zero line-length density (remnant vortices) of the order of 10–100 cm^{-2}. The existence of these remnant vortices may not be explained within this model. They can be, however, included by adding a small production term to the right-hand side of Eq. (38). We make this modification in Section 5 when analyze the growth of anisotropic tangle from remnant vortices during the formation of the plane Couette flow.

Let us note that for $\alpha = 0$, Eq. (38) with V_L given by (39) reduces to a continuity equation for L. This means that for $\alpha = 0$ the production or degradation of vortex lines may take place only at boundaries. In other words, Eq. (38) implies that, inside the volume, the quantized vortex line-length production or decay is due solely to the interaction with the normal component. This poses a limitation to the proposed model. It is expected that in the zero temperature limit the energy dissipation and vortex degradation occurs through phonon generation associated with either reconnections or the Kelvin-wave cascade [17,34,30]. This process may become dominant when the characteristic vortex line curvature is of the order of the inverse of the vortex core. Note that curvature coefficients c_1 and c_2 grow with decreasing α (Table 1). Some production of line-length density, in the absence of normal fluid can also take place due to the elongation of quantized vortex lines in superflow in dynamo-like mechanism. We have also neglected this effect by assuming that the macroscopic superfluid velocity $\mathbf{V}_s$ is constant across the small volume Ω. In normal fluids this

Table 1
Numerical values of dimensionless parameters characterizing quantum turbulence from Schwarz [8], kinematic viscosity $\nu_n = \eta/\rho_n$ [cm^2/s] and total specific density ρ_n [g/cm^3]

T (K)	1.07	1.26	1.62	2.01	2.15
ρ_n/ρ	0.013	0.039	0.174	0.576	0.886
ρ	0.145	0.145	0.145	0.146	0.146
ν_n	1.5×10^{-2}	3.0×10^{-3}	5.1×10^{-4}	1.8×10^{-4}	1.7×10^{-4}
α	0.010	0.030	0.100	0.300	1.00
c_1	2.86	1.99	1.45	1.04	0.72
c_2	3.40	2.44	1.82	1.42	1.15
I_o	0.151	0.225	0.316	0.433	0.496

vortex elongation mechanism enables the Kolmogorov–Richardson cascade, which transfers the energy from large to smaller eddies and thus implies the increase of vortex line-length. It is however very difficult, if possible, to calculate this vortex line-length elongation term since it depends to the whole geometry of the flow and thus cannot be express in terms of local geometrical coefficients defined in previous section.

At higher temperatures, however, we will see that the dissipative interaction of the two components provides quantum line-length generation strong enough to assure the coupling of the two components. In other words, the line-length production and degradation terms, which are missed in Eq. (38), and which should be added to explain the behavior of the quantum tangle at zero temperature limit are probably not as important at higher temperatures. In fact, the coupling of the two components observed over many length scales [31,32] may suggest that Kolmogorov–Richardson cascades observed in both fluids are not independent. As argued by Vinen and Niemela [33,34], at spatial scales larger than the average separation between quantized vortex lines, the superfluid and normal fluids should be coupled by the relatively small polarization of superfluid vortex lines. The criteria for the coupling of the two components will be discussed in Section 5, where we show that even for relatively small $\alpha = 0.01$ (corresponding to $T = 1.07$ K), the line length production due to the interaction with the normal component is strong enough to dissipatively couple the two components. The presence of normal fluid may not be neglected even at temperatures as low as 1 K, at which it constitutes of less than 1% of the total fluid, because at this low temperature its viscosity ν_n is very high. As a result, the overall viscosity $\nu = \nu_n \rho_n/\rho$ of the fluid is greater at $T = 1.07$ K than at $T = 2.15$ K.

3.2. The boundary and the initial conditions

In this section we consider the possible boundary conditions for system (34)–(41). Let ∂U be the boundary of the volume U. We confine ourselves to the case when the boundary is impermeable i.e. that there is no net flux of mass through it,

$$(\rho_s \mathbf{n} \cdot \mathbf{V}_s + \rho_n \mathbf{n} \cdot \mathbf{V}_n)|_{\partial U} = 0, \tag{43}$$

where $\mathbf{n}$ denotes the unit normal vector to the boundary, directed to the vessel. The normal and superfluid velocities must then satisfy,

$$\mathbf{n} \cdot \mathbf{V}_n = \frac{\dot{Q}}{\rho S T}, \qquad \mathbf{n} \cdot \mathbf{V}_s = -\frac{\rho_n \dot{Q}}{\rho_s \rho S T}, \tag{44}$$

where $\dot{Q}$ is the surface density of the heat current, T the temperature, and S the specific entropy. Besides, the normal, viscous component should satisfy no slip condition

$$\mathbf{n} \times \mathbf{V}_n|_{\partial U} = 0. \tag{45}$$

If there is no thermally induced flow then the condition (43) together with (45) simplifies to

$$\mathbf{n} \cdot \mathbf{V}_s|_{\partial U} = 0, \qquad \mathbf{V}_n|_{\partial U} = 0. \tag{46}$$

Eq. (39) implies that when $\nabla \times \mathbf{V}_s \neq 0$ the vortex tangle (and the superfluid vorticity) moves across the flow of superfluid component. This implies that the boundary conditions must include an additional boundary condition connected with the rate of generation (or annihilation) of vortex lines at the wall. We analyze this problem in more detail. First

note that the same problem is present in HBVK equations in which (see the next section for details) the velocity of vortex lines is

$$\mathbf{V}_L = \mathbf{V}_s + \alpha\widehat{\boldsymbol{\omega}}_s \times \mathbf{V}_{ns}. \tag{47}$$

In a flow such as spin-up in cylinder the second term of the left hand side of Eq. (39) is perpendicular to the boundary and transports the vortex lines (superfluid vorticity) towards the axis of the cylinder. In the HBVK model, in which there is no production of vortex lines inside the container, all the superfluid vorticity has to be generated on side the walls of the vessel. Peradzynski et al. [35] have assumed that vorticity is produced at the side walls with the flux

$$j = \mathbf{n}\cdot\mathbf{V}_L\boldsymbol{\omega}_s = \chi(V_b - V_s)^p, \tag{48}$$

where $V_b - V_s$ is the difference between the velocity of the wall and the superfluid velocity at the wall. The constants χ and p characterize interaction between the wall and the fluid. Assuming $\chi = 0$, one must conclude that angular superfluid velocity is determined by the initial value of vorticity. In particular, the superfluid component has to remain at rest if initially the superfluid vorticity is zero. Determination of constants χ and p, however, goes beyond the HBVK model; this is one of the weakness of this model. Note, however, that the situation is different when one stops the rotating cylinder, in this case $\mathbf{n}\cdot\mathbf{V}_L$ is negative, and the vorticity annihilates on the boundary.

In case of the system (34)–(41) the situation is somehow better, because Eq. (37) contains the line-length production term. Although the line-length can be generated in the volume, the total superfluid vorticity cannot. This observation follows from the fact that all vortex lines in the vessel are either closed or have their endpoints on the boundaries. The close vortices make no contribution to the total superfluid vorticity, and the contribution coming from unclosed vortices is determined by the position of their endpoints. Nevertheless, if the line-length is produced in the volume, the "positive" vorticity in the cylinder may result from the annihilation of the "negative" vorticity on boundaries. For example, when the vortex ring touches the boundary the two endpoints arise. The net contribution to the total vorticity will then grow with the distance between those two endpoints. This suggests that in our model the macroscopic superfluid vorticity may build up even without line generation on the boundary.

In addition to the vortex generation in the form (48), the vortices may be generated on the boundary due to at least two other processes:

(1) The vortices may pin to the small protrusions on the boundary and be elongated in the superfluid flow. The simulations of Schwarz [9] show that the pined vortex inclines being swept by the flow, until the angle between vortex and the boundary is so small that the vortex depins. Then it may continue its motion until being pinned to the next protrusion. The pinning–depinning process, causes that in average the vortex lines are not perpendicular to the boundary; the average angle Θ between the normal to the boundary and vortex lines at their end points depends on boundary roughness. For the perfectly smooth boundary $\Theta = 0$. Lipniacki [36] showed that, in the absence of normal component, the line-length productions rate (due to elongation of pinned vortices) is proportional to the value of superflow at the boundary, density of vortex end points and the $\sin\Theta$. The elongated vortices build the specific vortex boundary layer; this process may be dominant at very low temperatures when the $\rho_n/\rho_s \ll 1$ and the interaction via normal component is weaker. For further analysis, in order not to deal with too many physical effects at the same time, we assume that the boundary is perfectly smooth and there is no pinning, i.e. $\Theta = 0$.

(2) The vortices may be dragged out of the boundary by the superflow, if $\mathbf{n}\cdot\mathbf{V}_s > 0$. This is the case of heat transfers; vortices produced at one boundary, for which $\mathbf{n}\cdot\mathbf{V}_s > 0$, annihilate at the another for which $\mathbf{n}\cdot\mathbf{V}_s < 0$.

Now, we would like to focus on the case when $\mathbf{n}\cdot\mathbf{V}_s = \mathbf{n}\cdot\mathbf{V}_n = 0$ at the boundary. In addition to that we assume that there is no pinning. As we said before, there is no symmetry between generation and annihilation of vortices at boundary. Indeed, if $\mathbf{n}\cdot\mathbf{q}\times\mathbf{V}_{ns}|_{\partial U} < 0$, the vortices may annihilate on the boundary, but no additional condition for line-length is needed. If, however $\mathbf{n}\cdot\mathbf{q}\times\mathbf{V}_{ns}|_{\partial U} > 0$ the line-length density at boundary must be determined by a separate equation. In this case we postulate that the line-length density at the boundary L_B satisfies the Vinen equation with no drift term and the generation term twice smaller than inside the volume, i.e.

$$\frac{\partial L}{\partial t} = \frac{1}{2}\alpha I_0 c_1 |\mathbf{V}_{ns}| L_B^{3/2} - \beta\alpha {c_2}^2 L_B^2. \tag{49}$$

The "no drift" assumption, $\operatorname{div}(LV_L) = L\operatorname{div}V_L + L\operatorname{grad}V_L = 0$, reflects the observation that the tangle cannot be blown-out of the boundary. As a result, even if the term $L\operatorname{div}V_L$ at the boundary is large, the vortices are stretched rather then dragged out of the boundary. The generation term is assumed to be twice smaller because close to the

boundary only the half of lines may expand, while the second part, oppositely oriented, should annihilate on the boundary.

In the more general case, when $\mathbf{n}\cdot\mathbf{V}_s|_{\partial U}\neq 0$, the vortices may be dragged out by the superflow. This implies the boundary production (or annihilation) term $L\mathbf{n}\cdot\mathbf{V}_s|_{\partial U}$.

The initial conditions must determine $\mathbf{V}_s$, $\mathbf{V}_n$ and L in the whole volume. Since $q\leqslant 1$ the line-length density L must satisfy

$$L\geqslant\frac{|\nabla\times\mathbf{V}_s|}{\kappa}. \tag{50}$$

The above condition must be satisfied for any positive time. Since the evolution of L and $\mathbf{V}_s$ is determined by separate equations in the system (34)–(41), it is not a straightforward consequence of the initial condition.

3.3. HBVK equations

For laminar flows when vortices form an array of parallel lines the system (34)–(41) simplifies to the HBVK equations. For parallel vortices $q\equiv 1$, which implies the that generation and the decay terms in Vinen equation (38) vanish, we have

$$\frac{\partial L}{\partial t}=\operatorname{div}(L\mathbf{V}_L). \tag{51}$$

Moreover, the equation for L is no longer needed since for $q\equiv 1$, $L=|\nabla\times\mathbf{V}_s|/\kappa=|\boldsymbol{\omega}_s|/\kappa$, and the mutual friction force can be expressed as a function of $\mathbf{V}_n$ and $\mathbf{V}_s$ only

$$\mathbf{F}_{ns}=\alpha\rho_s\frac{\nabla\times\mathbf{V}_s}{|\nabla\times\mathbf{V}_s|}\times\big((\nabla\times\mathbf{V}_s)\times(\mathbf{V}_n-\mathbf{V}_s)\big). \tag{52}$$

Eq. (52) supplements the dynamic equations for $\mathbf{V}_n$ and $\mathbf{V}_s$:

$$\operatorname{div}\mathbf{V}_n=\operatorname{div}\mathbf{V}_s=0, \tag{53}$$

$$\rho_s\left(\frac{\partial\mathbf{V}_s}{\partial t}+\mathbf{V}_s\cdot\nabla\mathbf{V}_s\right)=-\nabla p_s-\mathbf{F}_{ns}, \tag{54}$$

$$\rho_n\left(\frac{\partial\mathbf{V}_n}{\partial t}+\mathbf{V}_n\cdot\nabla\mathbf{V}_n\right)=-\nabla p_n+\mathbf{F}_{ns}+\eta\Delta^2\mathbf{V}_n. \tag{55}$$

The system (52), (55) is known as Hall–Vinen–Bekarevich–Khalatnikov equations. The superfluid vorticity propagates with the same velocity as line-length,

$$\mathbf{V}_L=\mathbf{V}_s+\alpha\widehat{\boldsymbol{\omega}}_s\times\mathbf{V}_{ns}, \tag{56}$$

The last equation results from Eq. (39), but can also be obtained by taking the curl of Eq. (54) and using the equality $L=|\boldsymbol{\omega}_s|/\kappa$. Using Eq. (56) one can express the mutual friction $\mathbf{F}_{ns}$ in the alternative form

$$\mathbf{F}_{ns}=\rho_s\boldsymbol{\omega}_s\times(\mathbf{V}_L-\mathbf{V}_s). \tag{57}$$

4. The uniform steady rotation and counterflow

We consider the flow for which $\mathbf{V}_{ns}$, $\boldsymbol{\omega}_s$ and $\boldsymbol{\omega}_n$ are constant in space and time. The aim is to analyze the stationary, homogenous (invariant with respect to translations) but anisotropic quantum turbulence. Such rotating turbulence is expected close to the axis of the rotating channel with axial counterflow. It has been studied experimentally by Swanson et al. [37] twenty years ago. Recently, the rotating turbulence received a lot of attention; it has been studied in numerical simulation by Tsubota et al. [15,16], and phenomenologically by Jou and Mongovi [38]. In their experiment, Swanson et al. [37] found that at a given temperature there are two critical counterflow velocities $V_{c1}=C_1\Omega^{1/2}$ and $V_{c2}=C_2\Omega^{1/2}$, where, for $T=1.65$ K, $C_1=0.053\pm 0.006\ \mathrm{cm\,s^{-1/2}}$ and $C_2=0.118\pm 0.009\ \mathrm{cm\,s^{-1/2}}$. Below V_{c1} the line-length density does not grow with counterflow and is given purely by the magnitude of Ω. At V_{c1}, L rises sharply to a new flat region, and then rises again after V_{c2} going as V_{ns}^2. The authors associated the first transition with the Kelvin–Glaberson instability [39], an instability which initiates growth of Kelvin vortex waves. Because L

grows as V_{ns}^2, above V_{c2}, they proposed that V_{c2} is the velocity at which ordered array is transformed into a polarized turbulent tangle. A different interpretation of the second critical velocity is given by Tsubota et al. [16]. The authors suggest that for $V_{ns} > V_{c2}$ the vortex tangle undergoes so many reconnections that it becomes unpolarized. They conclude that the polarized tangle becomes unstable if $L < CV_{ns}$, where $C = 5 \times 10^4\ \mathrm{cm}^{-4}\,\mathrm{s}^2$ for $T = 1.65$ K. We do not share this hypothesis. In our opinion, the tangle polarization may not vanish due to reconnections. The anisotropy of the rotating tangle is $q = 2\Omega/\kappa L$, thus the tangle may not become fully isotropic for finite Ω. Moreover, the authors conclusion seems to be in contradiction with their own numerical simulation; Figs. 9B, 10B, 11B in [16] refer to rotating turbulence with $q = \langle s' \rangle_z \simeq 0.45$, $L \simeq 70\ \mathrm{cm}^{-2}$ and $V_{ns} = 0.08\ \mathrm{cm\,s}^{-1}$. This gives $70\ \mathrm{cm}^{-2} = L < CV_{ns} = 320\ \mathrm{cm}^{-2}$, which implies $V_{ns} > V_{c2}$, and still the numerical simulation show stable polarized turbulence. The counterflow velocity in Tsubota et al. [16] numerical simulation is also substantially larger than the second critical velocity $V_{c2} = C_2\Omega^{1/2} = 0.026\ \mathrm{cm\,s}^{-1}$ determined in the experiment by Swanson et al. [37]. This is why we would rather expect, as hypothesized by Swanson et al. [37] twenty years ago, and recently by Jou and Mongovi [38], that at V_{c2} the ordered array of lines undergo a transition into a turbulent polarized disordered tangle of interconnected vortices. And that this transition takes place through the reconnections of deformed helical lines when the amplitude of helical waves becomes of the order of vortex separation, as shown by numerical simulation by Tsubota et al. [16].

Since the integral in Eq. (18) vanish for close lines, there is no possibility that the anisotropic quantum tangle, $q > 0$, consists only of closed loops. In fact, as show numerical experiments based on LIA (Schwarz, Figs. 1, 4, 27, [8]) or based on Biot–Savart law (Tsubota et al., Fig. 6F [16]) even in the case of quasi isotropic tangle, $q \simeq 0$, closed loops are not very common even if the initial configuration consists only of rings. Simulations by Tsubota et al. [16] show that as polarization q grows (Fig. 6F, $q \simeq 0.2$ and Fig. 7F, $q \simeq 0.45$) vortex lines become more and more ordered in the direction of macroscopic vorticity, and do not suggest that vortex loops are abundant for any q. In the case of quantum turbulence in the rotating cylinder, the net number of vortex endpoints on bottom and upper wall (number of endpoints for which vortex goes out of the cylinder minus number of endpoints for which vortex goes into the cylinder) is given by the total macroscopic vorticity.

There is a natural temptation to describe the isotropic tangle as a gas of vortex rings or loops, with curvature of the order of $L^{1/2}$ (or the anisotropic tangle as a composition of loops and ordered lines). In our opinion this intuition is incorrect; Let us consider the decay of such a tangle after the counterflow is switched off. All rings will shrink, and because the speed of shrinking is proportional to the curvature, the process would speed-up as time goes. As a result the tangle will disappear in a finite (short) time. This is not observed; the tangle decay is at first fast, then gradual. This is possible, since the majority of vortices is of the form of long lines, with the endpoints on the boundaries. The shrinking of such lines causes their characteristic curvature to decrease (it remains of the order of $L^{1/2}$), what slows down the process. Eventually the tangle decay may end-up with a small number of remnant vortices (with low curvature) spanned between the walls of the vessel.

Tsubota et al. [16] analyzed the rise of rotating turbulence due to the applied counterflow from a set of parallel vortex lines. As one could expect the Kelvin–Glaberson instability induces helical waves on vortices. When the amplitude of the these waves becomes of the order of the average vortex separation, reconnections take place, and the anisotropic tangle develops. It would be interesting to simulate the other scenario; Let initially the temperature gradient sustain quasi isotropic turbulence, $q \simeq 0$. Then let the cylinder to rotate. The final picture should be the same – the anisotropic quantum tangle with $q > 0$. The simplest possibility is that the positive vorticity is generated at the side walls and then positively oriented lines migrate toward the center. However, if the walls are perfectly smooth (no pinning) the other possible scenario is that the negative vorticity is annihilated on the side walls. Namely, the Magnus force would push the positively oriented lines toward the center of cylinder, while negatively oriented lines would move outwards to the boundaries when they annihilate. Obviously the process must be quite complicated, and since lines are entangled it must involve many reconnections.

The model we proposed is far too simple to predict any of the two critical velocities: V_{c1} or V_{c2}. We expect, however, that it should provide a satisfactory description of the correlation between the angular velocity, counterflow and line-length density for polarized tangle in the regime above the second critical velocity V_{c2}.

Our aim is to compare our predictions with the experimental results of Swanson et al. [37] and theoretical predictions by Jou and Mongovi [38]. For a constant and uniform flow from the modified Vinen equation (38) one obtains

$$L = V_{ns}^2 \left(\frac{c_1\, I_0}{\beta\, c_2^2} \right)^2 \frac{1}{(1-q^2)^2} = \frac{L_H}{(1-(L_\omega/L)^2)^2}, \tag{58}$$

where L_H

$$L_H = V_{ns}^2 \left(\frac{c_1\, I_0}{\beta\, c_2^2} \right)^2 \tag{59}$$

is the steady-state line-length density resulting from same counterflow V_{ns} with $q = 0$ and, L_ω

$$L_\omega = \frac{\omega_s}{\kappa} = \frac{2\Omega}{\kappa} \tag{60}$$

is the line-length density associated with rotation ω_s and zero counterflow. As one should expect, for any $\lambda \geqslant 0$

$$L = (\lambda L_H, \lambda L_\omega) = \lambda L(L_H, L_\omega), \tag{61}$$

or when expressing L as a function of V_{ns} and Ω

$$L = \left(\lambda V_{ns}, \lambda^2 \Omega\right) = \lambda^2 L(V_{ns}, \Omega). \tag{62}$$

As a result it is enough to determine L as a function of L_H/L_ω, for given L_H or L_ω. Eq. (58) can be transformed into

$$L = L_H + \frac{2L_\omega}{L} - \frac{L_\omega^4}{L^3}. \tag{63}$$

Let us note also that for any L_H, L_ω there is a solution to Eq. (63) for which $L \geqslant L_\omega$ and $L \geqslant L_H$. While our model does not do this, the Jou and Mongovi [38] model distinguishes between the high counterflow regime $V_{ns} > V_{c2}$, and the low counterflow regime with $V_{ns} < V_{c2}$. In the case $V_{ns} > V_{c2}$ Jou and Mongovi [38] obtained (see Eq. (4.7) [38]; in Eq. (4.14) which follows from (4.7) there are two misprints: there is β^4 instead β_4 and terms in parentheses have wrong sign) the following expression for line-length density in rotating fluid with angular velocity Ω in presence of counterflow V_{ns}^2

$$L = \bar{\gamma}^2 V_{ns}^2 + \left(\frac{\beta_2}{\alpha_3} - \frac{\beta_4}{\alpha_1} \right)^2 \frac{\Omega}{\kappa} + 2\bar{\gamma} \left(\frac{\beta_2}{\alpha_3} - \frac{\beta_4}{\alpha_1} \right) V_{ns} \sqrt{\frac{\Omega}{\kappa}}. \tag{64}$$

The parameters appearing in the above equation were chosen based on experimental data from Swanson et al. [37], and according to Jou and Mongovi [38]: $\beta_2/\alpha_3 - \beta_4/\alpha_1 = 1.253$. Equality $\bar{\gamma} = \gamma_H$, where $\gamma_H^2 = L_H/V_{ns}^2$, would imply (see Eq. (6.11) [38]) that the binormal anisotropy vector $\mathbf{I}$ does not depend on the tangent anisotropy vector $\mathbf{q}$. We have made this simplifying assumption earlier in our model (see also Appendix A). The authors [38,40], however, state that the coefficient $\bar{\gamma}$ differs from γ_H. This implies that the equation may not be applied to the case $\Omega = 0$, and may suggest that there is some minimum value of Ω below which Eq. (64) is not valid [40]. In the case of high rotation, the authors [38,40] based on Fig. 1 of Swanson et al. [37] estimate the values of $\bar{\gamma} = 47\ \mathrm{s\,cm^{-1}}$ and $\gamma_H = 94\ \mathrm{s\,cm^{-1}}$, which implies $\bar{\gamma}/\gamma_H = 1/2$. Since $L_H = \bar{\gamma}^2 V_{ns}^2$, and $L_\omega = 2\Omega/\kappa$ one can rewrite Eq. (64) as follows

$$L = \left(\frac{\bar{\gamma}}{\gamma_H} \right)^2 L_H + 0.785 L_\omega + 1.772 \left(\frac{\bar{\gamma}}{\gamma_H} \right) \sqrt{L_H L \omega}. \tag{65}$$

In Table 2 we compare predictions of our implicit Eq. (63) and Eq. (65) both for $\bar{\gamma}/\gamma_H = 1$ and $\bar{\gamma}/\gamma_H = 1/2$ with the experiment by Swanson et al. [37] As we may observe the model we proposed reproduces the experimental data quite satisfactorily. Its main advantage is that to obtain expression (63) we do not introduce any free parameters, and that this expression is universal for all temperatures. Obviously, the experiments at other temperatures are needed in order to confirm the validity of Eq. (63). Due to its simplicity, the proposed model is applicable only to the case in which $V_{ns} > V_{c2}$ and may not describe the transitions at $V_{ns} = V_{c1}$ and $V_{ns} = V_{c2}$.

The fact that prediction of Eq. (65) depart substantially from the date of the Swanson [37] experiment implies that within the framework of Jou and Mongovi [38] model, that the ratio $\bar{\gamma}/\gamma_H$ cannot be assumed to be constant [40].

Now let us consider two limiting cases:

I. *Slow rotation and large counterflow*, $L_H \gg L_\omega$. In this limit the resulting line-length density L reads,

$$L = L_H \left(1 + 2 \left(\frac{L_\omega}{L_H} \right)^2 \right). \tag{66}$$

Table 2
The scaled line-length density L/L_ω as a function of L_H/L_ω. In the second row there are data from the Swanson [37] experiment (Figs. 2 and 3). The third row corresponds to our model with $(L/L_\omega)_L$ calculated from the implicit equation (63), the fourth row gives the value of $(L/L_\omega)_{J1}$ based on Eq. (65) for $\bar{\gamma}/\gamma_H = 1$, while the fifth row gives the value of $(L/L_\omega)_{J1/2}$ based on Eq. (65) for $\bar{\gamma}/\gamma_H = 1/2$. Let us note also that the Swanson measurements for $L_H/L_\omega \leqslant 0.4$ were done for a very small counterflow, $V_{ns}^2 \leqslant 0.2$ cm^2 s^{-2}, which is comparable with the critical counterflow V_{c2} at which the turbulence starts from an ordered array of lines

L_H/L_ω	9.61	5.41	2.91	1.54	0.86	0.4	0.2	0.1
$(L/L_\omega)_S$	9.70	5.60	3.35	2.25	1.85	1.45	1.20	1.04
$(L/L_\omega)_L$	9.81	5.75	3.46	2.32	1.80	1.45	1.28	1.19
$(L/L_\omega)_{J1}$	15.89	10.31	6.71	4.32	3.29	2.31	1.78	1.45
$(L/L_\omega)_{J1/2}$	5.93	4.19	3.02	2.27	1.82	1.45	1.23	1.09

Note that $L < L_H + L_\omega$ and even $(\mathrm{d}L/\mathrm{d}L_\omega) = 0$, at $L_\omega = 0$ which implies that in this limit the rotation only slightly modifies the density of tangle. It is quite intuitive since small polarization of a dense tangle can generate a sizable rotation, without significantly altering the tangle density.

II. *Large rotation and small counterflow*, $L_H \ll L_\omega$. Then the resulting line-length density L reads,

$$L = L_\omega\left(1 + \frac{1}{2}\left(\frac{L_H}{L_\omega}\right)^{1/2}\right). \tag{67}$$

In this case $L > L_H + L_\omega$ and $(\mathrm{d}L/\mathrm{d}L_H) = \infty$, at $L_H = 0$. This implies that even a small counterflow can generate turbulence when it is applied to an existing array of lines. This is in general agreement with the Swanson et al. [37] experiment (see Table 2) which, however, as already said, indicates that there is some critical value of the counterflow V_{c2} needed to turbulize the array of parallel vortices.

5. Formation of the plane Couette flow

In this section we consider the evolution of the boundary layer and the formation of the plane Couette flow. We analyze the flow between two material surfaces $z = 0$ and $z = D$. We will assume that the flow of the normal component remains laminar. This restricts our analysis to the relatively small $D\,V_0$, where V_0 is the characteristic velocity. Let us assume that for time $t < 0$,

$$\mathbf{V}_s \equiv 0, \quad \mathbf{V}_n \equiv 0, \quad \mathbf{q} \equiv 0, \quad L \equiv L_0, \tag{68}$$

where L_0 is the initial density of the remnant vortices. Then assume that at $t = 0$ the material plane $z = 0$ starts moving along the x axis with a constant velocity V_0. As a result, the following scenario may be expected: the normal component will start moving due to the viscosity forces. This introduces the velocity difference between normal and superfluids components i.e. the counterflow. The counterflow causes the line-length density to grow, and the two components become coupled by mutual friction. The fact that superfluid velocity tends to match with the normal velocity makes that $\boldsymbol{\omega}_s \neq 0$, which implies tangle polarization and its drift. After a sufficiently long time we may expect the formation of the shear flow. A similar problem of spin-up in an infinitely long cylinder has been already considered [41] within the framework of the Vinen model, i.e. using the classical Vinen equation, with no drift of the tangle included. The Vinen model, however, was found to be inconsistent: the line-length density calculated from the superfluid velocity profile was found to be greater than the total line density. Here we analyze the formation of the plane Couette flow by means of numerical simulations, using system (34)–(41), in which the last terms in Eq. (37), (39) proportional to I_0 are neglected. In this specific case Eqs. (34)–(41) simplifies to the system of scalar equations. Let

$$U := (\mathbf{V}_s)_x, \quad V := (\mathbf{V}_n)_x, \quad F := (\mathbf{F}_{ns})_x, \quad q := (\mathbf{q})_y, \quad W := (\mathbf{V}_L)_z, \tag{69}$$

where $(\cdot)_i$ denotes the ith component. The symmetry of the problem implies that the other components of $\mathbf{V}_s$, $\mathbf{V}_n$, $\mathbf{F}_{ns}$, $\mathbf{q}$ vanish, while the x component of $\mathbf{V}_L$ is not important. The parameter β (Eq. (9)) depends logarithmically on the average line curvature, but for typical densities of the tangle $\beta \approx \kappa$. Here for the sake of simplicity we put $\beta = \kappa$. We now have

$$\rho_s\left(\frac{\partial U}{\partial t}\right) = -F, \tag{70}$$

$$\rho_n\left(\frac{\partial V}{\partial t}\right) = F + \eta\frac{\partial^2 V}{\partial^2 z}, \tag{71}$$

with

$$F = \frac{2+q^2}{3}\alpha\kappa\rho_s L(U-V), \tag{72}$$

$$\frac{\partial L}{\partial t} = \alpha I_0 c_1\left(1-q^2\right)|V-U|L^{3/2} - \kappa\alpha {c_2}^2\left(1-q^2\right)^2 L^2 - \frac{\partial}{\partial z}(LW), \tag{73}$$

where

$$W = \alpha q(U-V), \qquad q = \frac{1}{\kappa L}\frac{\partial U}{\partial z}. \tag{74}$$

Let us now define the following characteristic measures needed to make the above system of equations nondimensional; turbulent line-length density scale L_H and rotational line-length density scale L_ω

$$L_H = V_0^2\left(\frac{c_1\ I_0}{\kappa\ c_2^2}\right)^2, \tag{75}$$

$$L_\omega = \frac{V_0}{\kappa D}. \tag{76}$$

Characteristic time scale of line-length density changes T_L, entrainment time scale T_{ns}, and normal velocity diffusion time scale T_D

$$T_L = \frac{1}{\kappa\alpha c_2^2 L_H}, \tag{77}$$

$$T_{ns} = \frac{1}{\kappa\alpha L_H}, \tag{78}$$

$$T_D = \frac{D^2}{\nu_n}, \qquad \nu_n = \frac{\eta}{\rho_n}. \tag{79}$$

The time scale T_L should not be confused with another time scale T_{prod}

$$T_{\text{prod}} = \frac{1}{\alpha I_0 c_1 V_0 L_0^{1/2}}, \tag{80}$$

in which the counterflow V_0 generates the tangle from the initial line-length density L_0. In typical situation $L_0 < L_H$ and $T_{\text{prod}} > T_L$.

Finally, let us recall time scale $T_R = \delta/v_l$, introduced by Schwarz [10], in which vortex-line tangent and the higher derivatives randomize. Since the typical interline spacing is $\delta = L^{-1/2}$ and average self-induced velocity is $v_l = \beta L^{-1/2}$

$$T_R = 1/\beta L. \tag{81}$$

It is important for our considerations that the time scale T_R is much shorter than T_{prod} and T_D (see Table 3) which determine time span of the process, so the tangle can be considered as relaxed. The assumption about local relaxation of the tangle is used in Appendix A where the distribution of the tangent $\mathbf{t} = \mathbf{s}'$ giving the prescribed anisotropy $\mathbf{q}$ is calculated.

Defining the scaled variables

$$u := \frac{U}{V_0}, \quad v := \frac{V}{V_0}, \quad l := \frac{L}{L_H} \tag{82}$$

we may rewrite Eqs. (70)–(74) as follows

Table 3
Parameters characterizing boundary layer and the formation of the shear flow, calculated for five various temperatures. All values are given for $D = 1$ cm, $V_0 = 1\ \mathrm{cm\,s^{-1}}$, while appropriate scaling is given in the last column. Time T_{prod} is calculated for $L_0 = 100\ \mathrm{cm^{-2}}$

T (K)	1.07	1.26	1.62	2.01	2.15	scaling
α	0.01	0.03	0.1	0.3	1.	~ 1
L_ω [cm^{-2}]	10^3	10^3	10^3	10^3	10^3	$\sim V_0/D$
T_L [s]	6.18	0.990	0.158	0.0331	0.0119	$\sim V_0^{-2}$
T_{ns} [s]	71.4	5.89	0.523	0.0668	0.0157	$\sim V_0^{-2}$
T_D [s]	66.7	333.	1.96×10^3	5.55×10^3	5.88×10^3	$\sim D^2$
T_{prod} [s]	23	6.7	2.2	0.74	0.28	$\sim V_0^{-1}$
T_R [s]	0.72	0.18	0.052	0.020	0.014	$\sim V_0^{-2}$
a_1	0.934	56.6	3.75×10^3	8.33×10^4	3.74×10^5	$\sim D^2\,V_0^2$
a_2	70.9	1.39×10^3	1.78×10^4	6.13×10^4	4.81×10^4	$\sim D^2\,V_0^2$
a_3	10.8	337.	1.24×10^4	1.68×10^5	4.94×10^5	$\sim D^2\,V_0^2$
a_4	0.476	1.767	10.25	33.36	92.3	~ 1
a_5	0.714	0.177	0.0523	0.0200	0.0157	$\sim D^{-1}\,V_0^{-1}$
$(DV_0)_{\mathrm{crit}}$	5 cm^2 s^{-1}	1 cm^2 s^{-1}	0.3 cm^2 s^{-1}	0.015 cm^2 s^{-1}	0.01 cm^2 s^{-1}	

$$\frac{\partial u}{\partial t} = \frac{l(v-u)}{T_{ns}}\left(\frac{2+q^2}{3}\right), \tag{83}$$

$$\frac{\partial v}{\partial t} = \frac{\rho_s l(u-v)}{\rho_n T_{ns}}\left(\frac{2+q^2}{3}\right) + \nu_n \frac{\partial^2 v}{\partial z^2}, \tag{84}$$

$$\frac{\partial l}{\partial t} = \frac{(1-q^2)\,l^{3/2}}{T_L}\left(|v-u| - \left(1-q^2\right)l^{1/2}\right) + \alpha V_0 \frac{\partial}{\partial z}\left(lq(v-u)\right), \tag{85}$$

$$q = \frac{\alpha V_0 T_{ns}}{l}\frac{\partial u}{\partial z}. \tag{86}$$

Now, introducing dimensionless time and space variables

$$\tau := \frac{t}{T_D}, \qquad \zeta := \frac{z}{D} \tag{87}$$

we obtain

$$\frac{\partial u}{\partial \tau} = \frac{l T_D(v-u)}{T_{ns}}\left(\frac{2+q^2}{3}\right), \tag{88}$$

$$\frac{\partial v}{\partial \tau} = \frac{\rho_s l T_D(u-v)}{\rho_n T_{ns}}\left(\frac{2+q^2}{3}\right) + \frac{\partial^2 v}{\partial \zeta^2}, \tag{89}$$

$$\frac{\partial l}{\partial \tau} = \frac{(1-q^2)T_D l^{3/2}}{T_L}\left(|v-u| - \left(1-q^2\right)l^{1/2}\right) + \frac{\alpha^2 V_0^2 T_D T_{ns}}{D^2}\frac{\partial}{\partial \zeta}\left(\frac{\partial u}{\partial \zeta}(v-u)\right), \tag{90}$$

$$q = \frac{\alpha\ V_0 T_{ns}}{Dl}\frac{\partial u}{\partial \zeta}. \tag{91}$$

Note, that the drift term in Eq. (90), calculated by substituting q from Eq. (91) does not depend explicitly on l. The dynamics of the system depends on five dimensionless constants

$$a_1 = \frac{T_D}{T_{ns}}, \quad a_2 = \frac{\rho_s T_D}{\rho_n T_{ns}}, \quad a_3 = \frac{T_D}{T_L},$$
$$a_4 = \frac{\alpha^2 V_0^2 T_D T_{ns}}{D^2}, \qquad a_5 = \frac{\alpha\ V_0\ T_{ns}}{D}. \tag{92}$$

Note that $a_4 = a_1 a_5^2$, which assures that for $q = 1$ the line-length density propagates with the same velocity as superfluid vorticity. Finally our system takes the following form

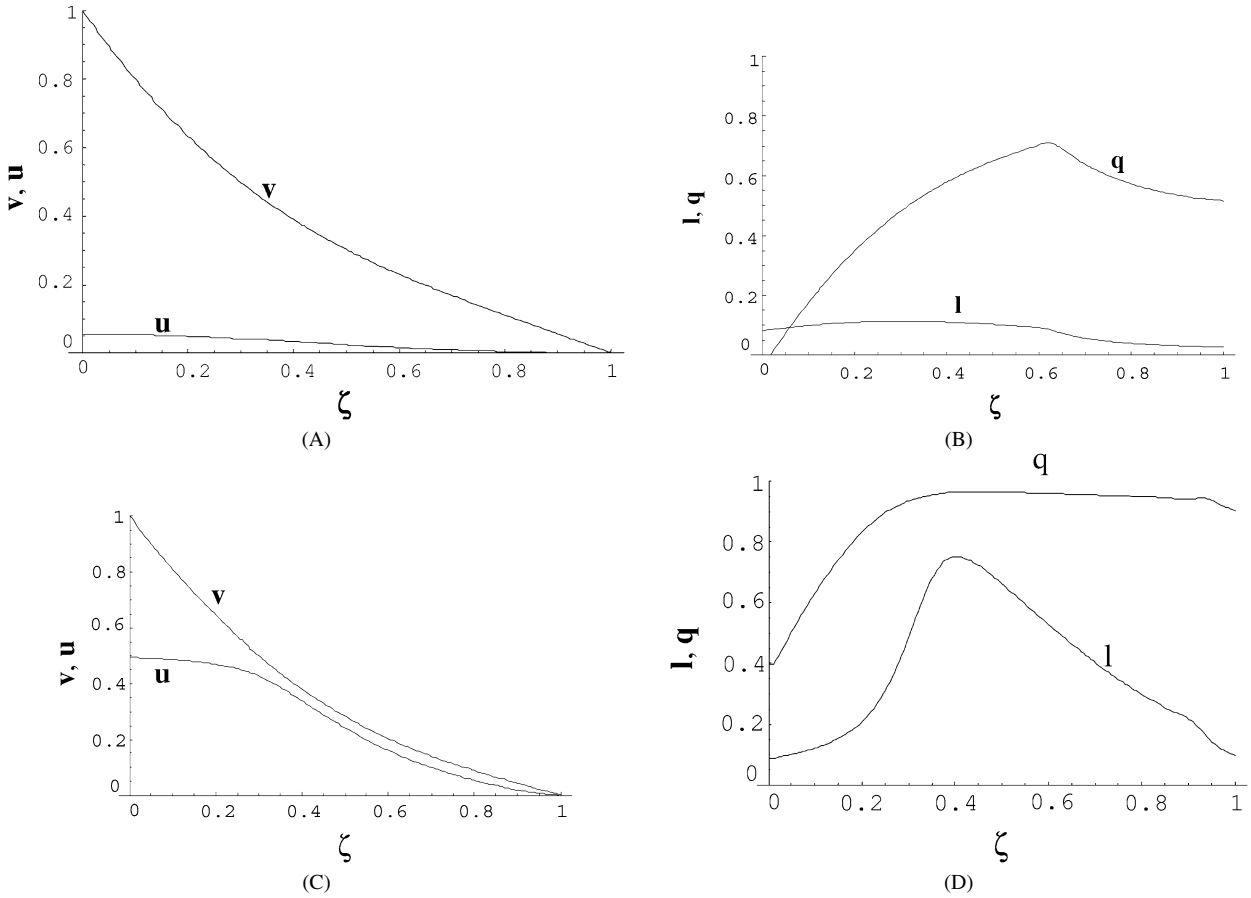

Fig. 1. Formation of plane Couette flow at $T = 1.07$ K ($\alpha = 0.01$) with $D\,V_0 = 1\ \mathrm{cm^2\,s^{-1}}$. Panel A: normal and superfluid velocity profiles, and Panel B: line-length density l and anisotropy coefficient q at $\tau = 2$. Panels C and D: the same flow at $\tau = 10$.

$$\frac{\partial u}{\partial \tau} = a_1 l(v-u)\left(\frac{2+q^2}{3}\right), \tag{93}$$

$$\frac{\partial v}{\partial \tau} = a_2 l(u-v)\left(\frac{2+q^2}{3}\right) + \frac{\partial^2 v}{\partial \zeta^2}, \tag{94}$$

$$\frac{\partial l}{\partial \tau} = a_3\big(1-q^2\big)l^{3/2}\big(|v-u| - \big(1-q^2\big)l^{1/2}\big) + a_4\frac{\partial}{\partial \zeta}\left(\frac{\partial u}{\partial \zeta}(v-u)\right) + a_3 l_0^2, \tag{95}$$

$$q = \frac{a_5}{l}\frac{\partial u}{\partial \zeta}. \tag{96}$$

In order to maintain some non-zero density l_0 of remnant vortices in the region before the tangle front we added to Eq. (95) the second generation term equal $a_3\ l_0^2$. With this term the system of Eqs. (93)–(96) possesses the stable solution $u_i \equiv 0$, $v_i \equiv 0$, $l \equiv l_0$. This additional term not only assures that line density does not drop to zero, but also increases the numerical stability of the system. In numerical simulations we set $l_0 = 0.02$.

We make use of the following boundary conditions:

$$v(1) = 0, \qquad v(0) = 1. \tag{97}$$

The line-length l_B at the boundary $\zeta = 0$ will be calculated based on (49), which in dimensionless variables takes the form

$$\frac{\partial l}{\partial \tau} = a_3 l^{3/2}\left(\frac{|v-u|}{2} - l^{1/2}\right) + a_3 l_0^2, \tag{98}$$

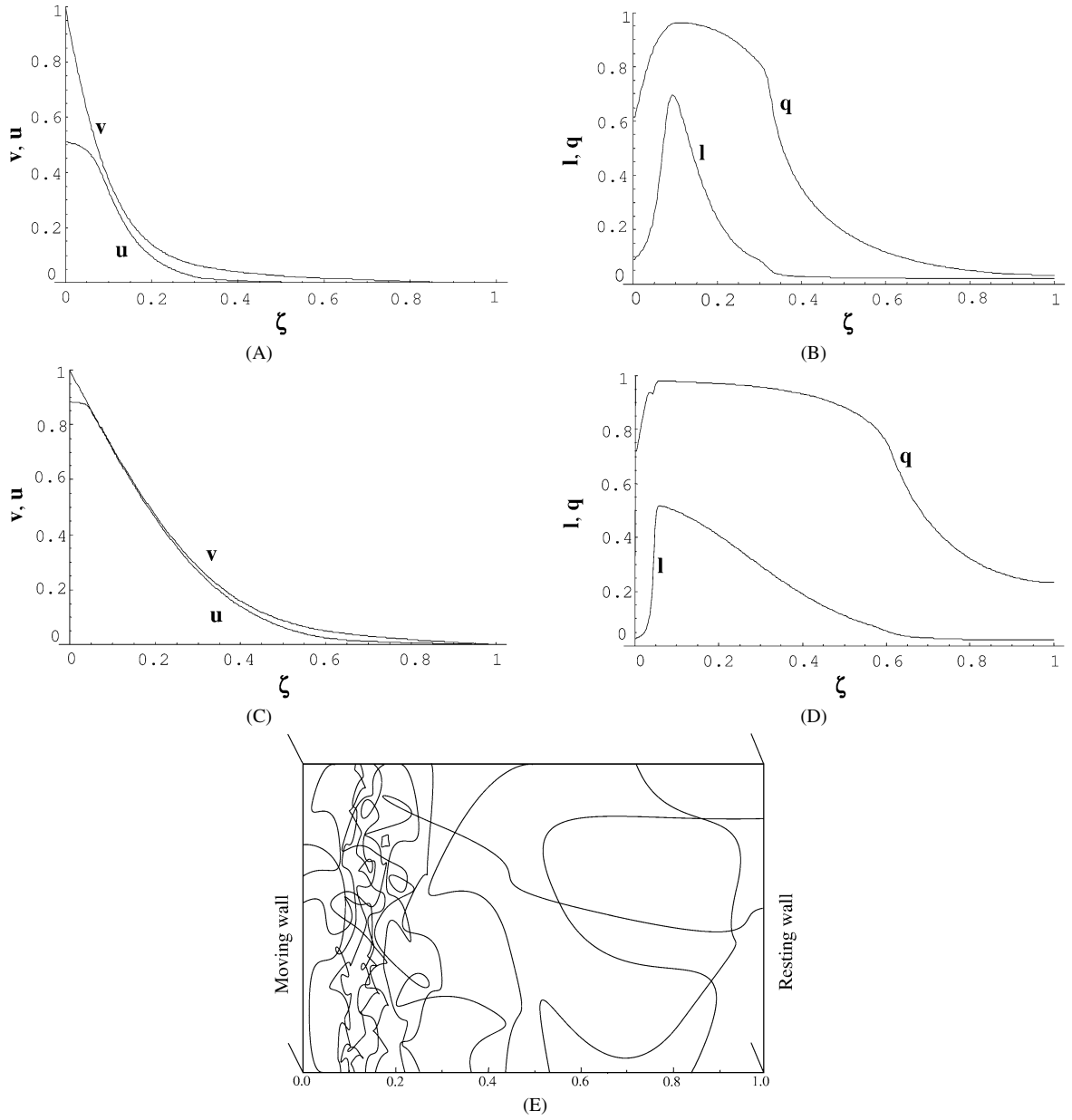

Fig. 2. Formation of plane Couette flow at $T = 1.26$ K ($\alpha = 0.03$) with $DV_0 = 1$ cm^2 s^{-1}. Panel A: normal and superfluid velocity profiles, and Panel B: line-length density l and anisotropy coefficient q at $\tau = 0.2$. Panels C and D: the same flow at $\tau = 1$. Panel E: a schematic graph showing the hypothetical arrangement of quantum vortex lines in the flow shown in Panels A and B; view in the direction of normal and superfluid velocity.

The initial conditions corresponding to formation of the Couette flow from the rest are

$$u_i \equiv 0, \quad v_i \equiv 0, \quad l_i \equiv l_0. \tag{99}$$

We have performed a number of numerical simulations of the system (93)–(96) for various sets of parameters a_1, a_2, a_3, a_4 and a_5, corresponding to different temperatures (see Table 3), and different DV_0. Note that for a given temperature it is only DV_0, not D and V_0 separately, that determines the parameters a_i. This resembles the classical fluid dynamics, where the character of the flow is governed by Reynolds number $Re = DV_0/\nu$. First, we discuss the evolution of the line-length density and the velocity profiles of both components at temperatures $T = 1.07$ K, $T = 1.26$ K and 1.62 K, with $DV_0 = 1$ cm^2 s^{-1}. In Fig. 1 we present line-length density l anisotropy parameter q,

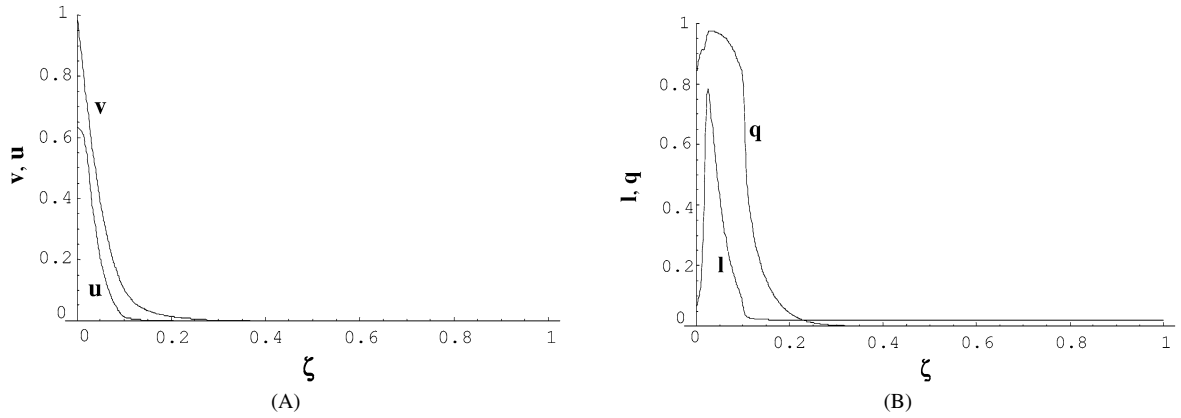

Fig. 3. Formation of plane Couette flow at $T = 1.64$ K ($\alpha = 0.1$) with $DV_0 = 1$ cm^2 s^{-1}. Panel A: normal and superfluid velocity profiles, and Panel B: line-length density l and anisotropy coefficient q at $\tau = 0.005$.

as well as normal and superfluid velocity profiles at times $\tau = 2$ and $\tau = 10$. Because the coupling between normal and superfluid is low, first the normal fluid velocity profile is set-up, then the counterflow gives rise to quantum turbulence, which slowly couples the two components. One can observe a very characteristic feature (Fig. 1C), either the velocity profiles of both components match, or, in the region where they do not match, the superfluid velocity is almost constant. In the last region, there are simply very few superfluid vortices, which are swept by the Magnus force towards the region where the velocities of the two components match. The quantum vortices are much more abundant in the region where the velocities match. In this region the vortices form ordered array and the anisotropy parameter q is large. The vorticity production occurs most efficiently at the place where these two regions meet. Such behavior is in close agreement, with the observation made by Samuels [42] who analyzed the velocity matching in pipe flow, using the Biot–Savart law to simulate quantum vortices; see Figs. 7 and 9 in his work. Similar profiles can be observed for $T = 1.26$ K (Fig. 2). Now, however, the coupling between the two components is stronger, and thus the region in which their velocities differ is much smaller. The time scale in which the components couple is comparable with the scale in which the normal component takes its velocity profile. In Fig. 2E we show the hypothetical configuration of vortex lines corresponding to the line-length density L and the anisotropy q shown in Fig. 2B. The view is in the direction of the normal and the superfluid velocity. Obviously, in the infinitely long channel we should see infinitely many vortices, but we draw only "one layer" of them. The vortices terminate on the left and the right walls, but continue up and down from the section shown. The Magnus force makes that the vortices move to the right, toward the region where the normal and superfluid velocities match. In this region, the small counterflow may not sustain turbulence and the vortices become ordered. Farther to the right, the normal and superfluid velocities are negligible, as a result there are only few unordered remnant vortices of small curvature.

For 1.62 K and $DV_0 = 1$ cm^2 s^{-1} (Fig. 3) the components couple very quickly, and then their velocity profiles evolve together until the Couette flow is reached. In this case the entrainment approximation, i.e. approximation in which one assumes that both components are locked together and move as a classical fluid with overall kinematic viscosity $\nu = \nu_n \rho_n / \rho$, is justified.

In Figs. 4 and 5 we show how the dynamics depends on the value of DV_0. In Figs. 4A and 4B we show velocity profiles, line-length density and anisotropy for the same temperature as in Fig. 3, i.e. 1.62 K, but for $DV_0 = 0.1$ cm^2 s^{-2}. In Figs. 4C and 4D we present line-length density and anisotropy for 1.07 K, same as in Fig. 1, but for $DV_0 = 20$ cm^2 s^{-1}. At the higher temperatures of 2.01 K and 2.15 K we present two types of flow for large and small DV_0 (Fig. 5). This shows that for each temperature there exist two regimes of the flow; the "entrainment regime"(Figs 3, 4C, D and 5B, D) – in which the fluids are locked together – for large DV_0, and (let us call it) the "low velocity regime" (Figs. 1, 2, 4A, B and 5A, C) – in which the superfluid and normal component velocity profiles are essentially different – for small DV_0. The flow regime depends on the initial line-length density and parameters a_1, a_2, a_3, a_4, a_5, which themselves depend on the temperature and DV_0. As a result, it is not straightforward how to determine analytically at what value of DV_0 the flow changes its character for a given temperature, especially that there is no sharp transition between these two flow regimes. We define the critical value $(DV_0)_{\text{crit}}$ as a value at which the width of the plateau of the superfluid velocity flow equals $D/10$ at the time when $V_s(0) = V_0/2$. According to this arbitrary definition the

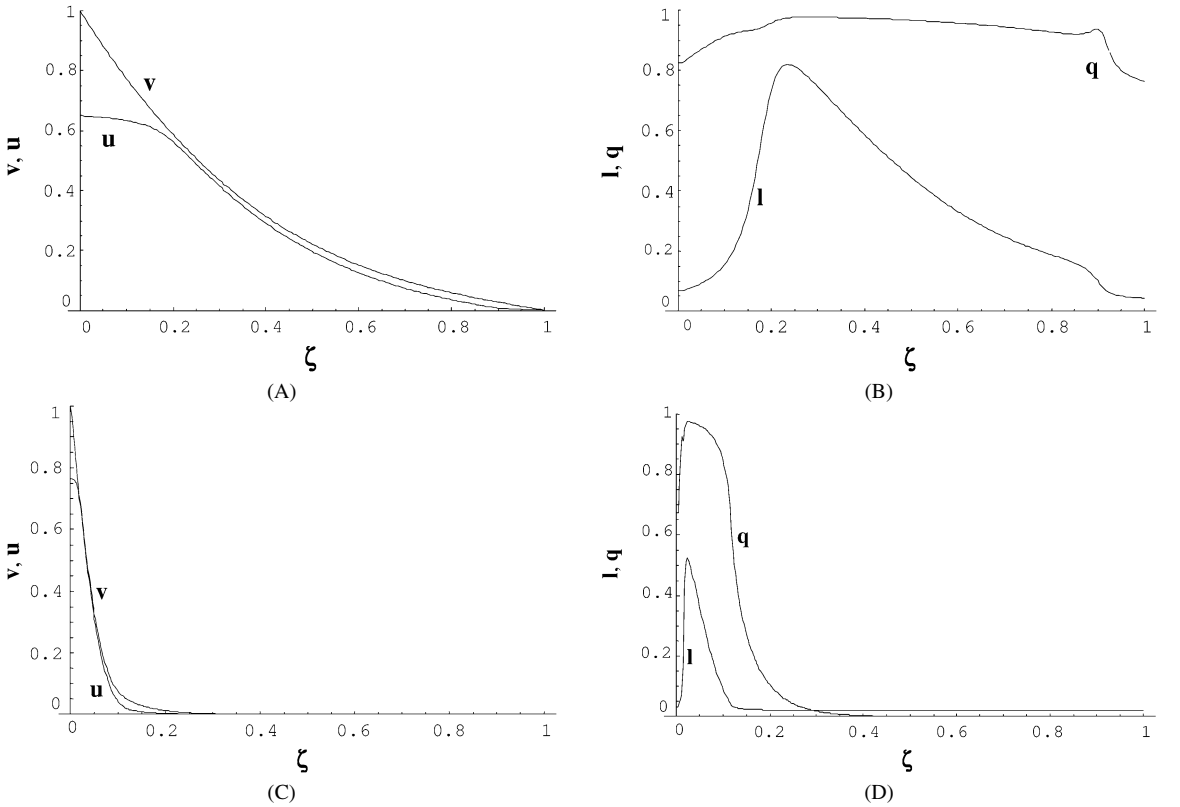

Fig. 4. Formation of plane Couette flow. Panels A and B correspond to $T = 1.62$ K ($\alpha = 0.1$), with $D V_0 = 0.1$ cm^2 s^{-1}, and $\tau = 1$. Panels C and D correspond to $T = 1.07$ K ($\alpha = 0.01$) and $D V_0 = 20$ cm^2 s^{-1}, and $\tau = 0.1$.

flow shown in Fig. 2A corresponds to the critical DV_0. Above the critical DV_0, the normal and superfluid flows can be considered as locked together. The characteristic transition values of DV_0 deduced form numerical simulations are given in Table 3. The critical value of DV_0 would be somewhat smaller for the larger initial line-length density. This in part supports the argument put forth by Vinen [33] and the Barenghi et al. [43] that polarization of a vortex tangle should correlate normal and superfluid velocity fields. Barenghi et al. [43] concluded, that provided that enough vortex lines are present, vorticity matching should take place over the entire inertial range. Our modeling and numerical simulations put this in more quantitative terms, showing the value of DV_0, (for a given temperature) above which the superfluid and normal-fluid flows are locked. We show also that in many cases the polarization of the tangle is very high.

Finally, we should compare the dynamics governed by the system (93)–(96) with a simpler model in which the evolution line-length density is described by the classical Vinen equation, which in the scaled variables (including the additional generation term) reads

$$\frac{\partial l}{\partial \tau} = a_3 l^{3/2}\big(|v-u| - l^{1/2}\big) + a_3 l_0^2. \tag{100}$$

In Eqs. (93) and (94) we set $q = 0$. The simulation is done for $T = 1.26$ K, with $DV_0 = 1$ cm^2 s^{-1}, so it should be compared with that of Fig. 2. During the simulation we keep $q = 0$ and then, after the simulation is done, having the line-length density and superfluid velocity profile, we calculate the anisotropy parameter q. If q would remain much smaller than 1, then the neglected tangle drift would be small and the classical Vinen description would be adequate. However, in the region of large superfluid vorticity, one obtains unphysical $q > 1$, see Fig. 6, which implies that the description of quantum tangle in formation of plane Couette flow via the classical Vinen is evidently inconsistent, and thus cannot produce correct velocity profiles. The line-length density following from the Vinen equation is smaller than the line-length density associated with the macroscopic superfluid vorticity calculated from the superfluid velocity profile.

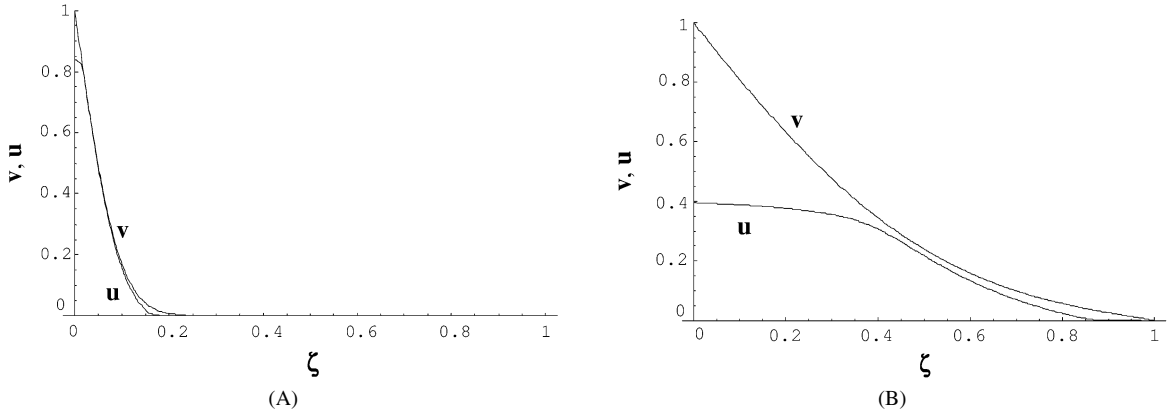

Fig. 5. Formation of plane Couette flow close to λ point ($T = 2.15$ K, $\alpha = 1$) for two values of DV_0. Panel 5A: $DV_0 = 0.02$ cm^2 s^{-1}, Panel 5B: $DV_0 = 0.2$ cm^2 s^{-1}.

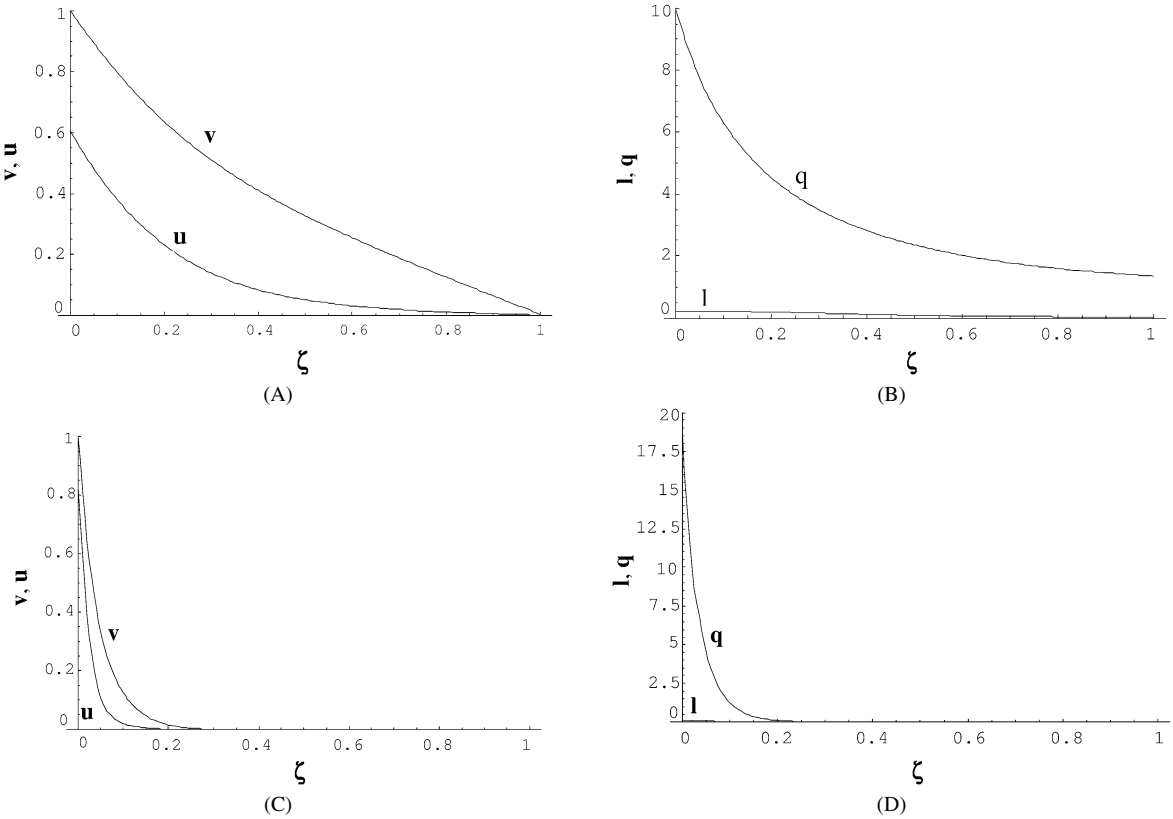

Fig. 6. Normal and superfluid velocity profiles, the line-length density l and the anisotropy coefficient q, during the formation of Couette flow in the case when the evolution of the line-length density is governed by the classical Vinen equation with the drift term neglected; Panels 6A and 6B: $T = 1.07$ K ($\alpha = 0.01$), $DV_0 = 1$ cm^2 s^{-1}, $\tau = 5$ and Panels 6C and 6D: $T = 1.62$ K ($\alpha = 0.1$), $DV_0 = 1$ cm^2 s^{-1}, $\tau = 0.005$. Note that, for both temperatures, the anisotropy coefficient q (Panels 6B and 6D) is greater than 1, which shows that the model is inconsistent.

6. Conclusions

In the paper we used the two scale approach to derive a system of equations describing the coupled dynamics of both helium components, together with the evolution of quantum tangle. In the microscopic scale we considered the dynamics of quantum vortex lines in order to generalize the Vinen equation to the case in which the tangle is not

isotropic but carries a significant macroscopic vorticity and the quantum lines are partially ordered in a given local direction. The anisotropy of the tangle results in the presence of the drift term in the modified Vinen equation, which describes the motion of the tangle across the counterflow. It also introduces the modification to the generation and decay terms in this equation. The flows of the normal and superfluid components are described by Navier–Stokes and Euler equations, respectively. Both equations are coupled by the drag force, proportional to the counterflow and relative velocity of the components.

The derived system has two previously explored limit cases. In the limit of the very small macroscopic superfluid vorticity, the quantum tangle is not polarized, and the classical Vinen equation, with no drift term can be applied. In this limit only the thermally induced counterflow can be analyzed. In the other limit the vortices form a locally parallel array of lines; the generation and decay of lines take place only on boundaries. This case, described by HBVK equations, is restricted only to the very small counterflow ($\mathbf{V}_{ns} < V_{c2}$), too slow to generate quantum turbulence.

The proposed system is applicable to much more general situations in which the flow of superfluid component is turbulent and anisotropic. This case has been intensively studied in the last two decades, in various experiments with mechanically generated turbulence [4–6]. It is, however, limited to the finite temperatures, at which $\alpha > 0$, since the "in volume" vortex line-generation and degradation, as described by the modified Vinen equation (38), is due solely to the interaction with normal fluid.

We applied the proposed model to two relatively simple flows.

First, we found that the line-length densities in the steady state turbulence in rotating vessel, calculated from our model, are in a satisfactory agreement with the experiment [37]. The main advantage of our prediction, Eq. (63), is the lack of free parameters which have to be fitted based on experiment.

Second, we analyzed the formation of the plane Couette flow. The numerical calculations indicate that there are two characteristic regimes. At a given temperature, the dynamics of the two helium components depends on DV_0, where D is the spatial scale of the flow and V_0 is the characteristic velocity.

I – For large DV_0 the characteristic time of tangle generation is shorter than the normal component diffusion scale. As a result, the fluids become locked together before the shear profile is achieved.

II – For small DV_0, the line generation is slow and the tangle is highly polarized. There are two characteristic regions in the flow, in one of them the counterflow is almost zero and the quantum vortices form an ordered array of lines, in the other counterflow is non-zero, but there are few vortices. The vortices are mainly generated in narrow layer where these two regions meet. The Magnus force makes that these vortices are swept toward the region where the normal and the superfluid velocities match. In this region, the small counterflow may not sustain the turbulence and the vortices become ordered.

In our considerations (see also Appendix) we assumed that the anisotropy vectors $\mathbf{q}$ and $\mathbf{I}$, describing respectively anisotropy of the tangent and binormal to the vortex lines in the tangle are independent. The main reason for this assumption is its simplicity. We see, however, the need for more a complex theory which would describe the co-evolution of anisotropy vectors and line-length density.

The proposed model is constructed for the superfluid ^{4}He (for this superfluid the data is the most accessible), we expect, however, that after slight modifications it may describe the superfluid ^{3}He. In this case the situation can be even better, since the normal component of ^{3}He is much more viscous than the normal component of ^{4}He, which implies that our assumption that the normal flow remains laminar is satisfied for larger DV_0.

Acknowledgements

I would like to thank Professor Zbigniew Peradzynski for helpful discussion.

Appendix A

To estimate $\mathbf{I}_v$ as a function of $\mathbf{q}$ and $\mathbf{V}_{ns}$, but also to show that the choice $\bar{c}_1(q) = c_1(1-q^2)$, $\bar{c}_2(q) = c_2(1-q^2)$, made in Section 2.3 is reasonable, we assume that the angular distribution $f_q(\mathbf{t})$ of unit tangent $\mathbf{t} = \mathbf{s}'$ to vortex lines in a volume Ω is the most probable distribution which results in a given $\mathbf{q}$ i.e.

$$\mathbf{q} = \frac{\oint f_q(\mathbf{t})\mathbf{t}\,\mathrm{d}\mathbf{t}}{\oint f_q(\mathbf{t})\,\mathrm{d}\mathbf{t}}, \tag{101}$$

where the integrals are taken over the unit sphere. This is quite a crude assumption, since we know that, in general, the distribution of the binormal $\mathbf{b} = \mathbf{s}' \times \mathbf{s}''$ is not uniform, and that the binormal is correlated with the tangent. The next step would be to look for the most probable distribution of the tangent which gives the prescribed $\mathbf{q}$ and $\mathbf{I}$; this, however, seems to be much more difficult.

As already said, all derivatives of vortex line randomize in time of order $T_R = \delta/v_l \simeq 1/\beta L$. This gives the characteristic time scale in which the distribution of the tangent becomes the most probable distribution satisfying the constraint (101). As shown in Table 3, time T_R is at least one order of magnitude shorter than time T_{prod} (time needed for build-up of a vortex tangle) or time T_D (in which the profile of normal velocity is set-up). It means that at least in the case considered in Section 5 (and obviously in the case from Section 4 where the steady-state rotating turbulence is considered) the tangle has enough time randomize.

The calculation of $f_q(\mathbf{t})$ is analogous to the one in our previous paper [21], and we obtain

$$f_q(\mathbf{t}) = C\mathrm{Exp}(\gamma \hat{\mathbf{q}} \cdot \mathbf{t}), \tag{102}$$

where $\hat{\mathbf{q}} = \mathbf{q}/q$, and γ is given implicitly by the following formula:

$$q = \frac{1 + \gamma + \mathrm{e}^{2\gamma}(\gamma - 1)}{-\gamma + \gamma \mathrm{e}^{2\gamma}}. \tag{103}$$

Let $\mathbf{t}_a$, $\mathbf{t}_b$ denote the unit tangent vectors to the vortex line at points a and b. If the distance between these two points is equal to the correlation length for the tangent, one may expect that $\mathbf{t}_a$ and $\mathbf{t}_b$ are weakly correlated and that the total line curvature between these points is roughly equal to the angle ϕ_{ab} between $\mathbf{t}_a$ and $\mathbf{t}_b$. Note that for uncorrelated $\mathbf{t}_a$, $\mathbf{t}_b$ we have

$$\langle \mathbf{t}_a \cdot \mathbf{t}_b \rangle = \langle \mathbf{t}_a \rangle \cdot \langle \mathbf{t}_b \rangle = \mathbf{q} \cdot \mathbf{q} = q^2. \tag{104}$$

Since $\alpha_{ab} = \arccos(\mathbf{t}_a \cdot \mathbf{t}_b)$, the average α_{ab} can be estimated as function of q

$$\langle \alpha_{ab} \rangle_q = \arccos\bigl(q^2\bigr) = \frac{\pi}{2} - q^2 - \frac{q^6}{6} - \frac{3q^{10}}{40} - \cdots. \tag{105}$$

We see that the average α_{ab} decreases with q and we have

$$\frac{\bar{c}_1(q)}{c_1} = \frac{\langle \alpha_{ab} \rangle_q}{\langle \alpha_{ab} \rangle_0} = \frac{\langle \alpha_{ab} \rangle_q}{\pi/2} = 1 - \frac{2q^2}{\pi} - \frac{q^6}{3\pi} - \frac{3q^{10}}{20\pi} - \cdots \approx 1 - q^2. \tag{106}$$

This suggests that the choice $\bar{c}_1(q) = c_1(1 - q^2)$, $\bar{c}_2(q) = c_2(1 - q^2)$ is reasonable.

Now we estimate $\mathbf{I}_v$. With out loss of generality we may assume that (in the considered volume Ω), vector $\mathbf{q}$ is along z axis. Let $\mathbf{V}_{ns} = \mathbf{V}_{\parallel} + \mathbf{V}_{\perp}$, where $\mathbf{V}_{\parallel}$ is parallel to $\mathbf{q}$ and $\mathbf{V}_{\perp}$ is perpendicular to $\mathbf{q}$. Then $\mathbf{I}_v$ reads

$$\mathbf{I}_v = \frac{1}{\Omega L} g \left(\int \mathbf{t}(\mathbf{t} \cdot \mathbf{V}_{\parallel})\, \mathrm{d}\xi + \int \mathbf{t}(\mathbf{t} \cdot \mathbf{V}_{\perp})\, \mathrm{d}\xi\, g \right), \tag{107}$$

and because of the rotational symmetry of the distribution $f(\mathbf{t})$ with respect to z axis we have

$$\mathbf{I}_v = \mathbf{V}_{\parallel} \langle t_z^2 \rangle + \mathbf{V}_{\perp} \langle t_x^2 \rangle. \tag{108}$$

Since $\langle t_x^2 \rangle + \langle t_y^2 \rangle + \langle t_z^2 \rangle = 1$ and because of the symmetry $\langle t_x^2 \rangle = \langle t_y^2 \rangle$, we have $\langle t_x^2 \rangle = (1 - \langle t_z^2 \rangle)/2$, so we need only to calculate $\langle t_z^2 \rangle$.

$$\langle t_z^2 \rangle_\gamma = \frac{\oint \mathrm{e}^{\gamma t_z}\, t_z^2\, \mathrm{d}t_z}{\oint \mathrm{e}^{\gamma t_z}\, \mathrm{d}t_z}, \tag{109}$$

$$\bigl\langle t_z^2 \bigr\rangle_\gamma = \frac{\int_0^\pi \sin(\Theta)\, \mathrm{e}^{\gamma \cos(\Theta)} \cos^2(\theta)\, \mathrm{d}\Theta}{\int_0^\pi \sin(\Theta)\, \mathrm{e}^{\gamma \cos(\Theta)}\, \mathrm{d}\Theta}, \tag{110}$$

$$\bigl\langle t_z^2 \bigr\rangle_\gamma = 1 + 2\frac{1 + \gamma + \mathrm{e}^{2\gamma}(\gamma - 1)}{\gamma^2(1 - \gamma\, \mathrm{e}^{2\gamma})} = 1 - \frac{2q}{\gamma}. \tag{111}$$

To have $\langle t_z^2 \rangle$ as a function of q instead of γ we use Eq. (103) and expand q with respect to γ; $q = b/3 - b^3/45 + 2b^5/945 + \mathrm{O}(b^7)$. This gives

$$\langle t_z^2 \rangle_q = \frac{1}{3} + \frac{2q^2}{5} + \frac{24q^4}{175} + \mathrm{O}(q^6). \tag{112}$$

Since we know that $\langle t_z^2 \rangle_q = 1$ for $q = 1$, we take $\langle t_z^2 \rangle_q = 1/3 + 2q^2/3$ to simplify further calculations. This gives $\langle t_x^2 \rangle_q = 1/3 - q^2/3$. Finally we have

$$\mathbf{I}_v = \mathbf{V}_\parallel \frac{1 + 2q^2}{3} + \mathbf{V}_\perp \frac{1 - q^2}{3}. \tag{113}$$

The above yields,

$$\mathbf{I}_v = \mathbf{q}(\mathbf{q} \cdot \mathbf{V}_{ns}) + \mathbf{V}_{ns}\left(\frac{1 - q^2}{3}\right) = \mathbf{q} \times (\mathbf{q} \times \mathbf{V}_{ns}) + \mathbf{V}_{ns}\left(\frac{1 + 2q^2}{3}\right). \tag{114}$$

References

[1] R.J. Donnelly, Quantized Vortices in Helium II, Cambridge University Press, 1991.
[2] R.J. Donnelly, Quantized vortices and turbulence in helium II, Annu. Rev. Fluid Mech. 25 (1993) 325.
[3] S.K. Niemirowski, W. Fiszdon, Chaotic quantized vortices and hydrodynamic processes in superfluid helium, Rev. Modern Phys. 67 (1995) 37.
[4] F. Belert, G. Stamm, Visualization of Taylor–Couette flow in superfluid helium, Cryogenics 33 (1993) 938.
[5] J. Maurer, P. Tabeling, Local investigation of superfluid turbulence, Europhys. Lett. 43 (1998) 29.
[6] M.R. Smith, R.J. Donnelly, N. Goldenfeld, W.F. Vinen, Decay of vorticity in homogeneous turbulence, Phys. Rev. Lett. 71 (1993) 2583.
[7] C.F. Barenghi, C.E. Swanson, R. J Donnelly, Emerging issues in helium turbulence, J. Low Temp. Phys. 100 (1995) 385.
[8] K.W. Schwarz, Three-dimensional vortex dynamics in superfluid ^{4}He: Homogenous superfluid turbulence, Phys. Rev. B 38 (1988) 2398.
[9] K.W. Schwarz, Three-dimensional vortex dynamics in superfluid ^{4}He: Line–line and line–boundary interactions, Phys. Rev. B 31 (1985) 5782.
[10] K.W. Schwarz, Turbulence in superfluid helium: Steady homogenous counterflow, Phys. Rev. B 18 (1978) 245.
[11] D.J. Melotte, C.F. Barenghi, Transition to normal fluid turbulence in helium II, Phys. Rev. Lett. 80 (1998) 4181.
[12] P.G. Saffman, Vortex Dynamics, Cambridge University Press, Cambridge, 1992.
[13] I.L. Bekarevich, I.M. Khalatnikov, Phenomenological derivation of the equations of vortex motion in He II, Sov. Phys. JETP 13 (1961) 643.
[14] M. Tsubota, T. Araki, S.K. Nemirowskii, Dynamics of vortex tangle without mutual friction in superfluid He-4, Phys. Rev. B. 62 (2000) 11751.
[15] M. Tsubota, T. Araki, C.F. Barenghi, Rotating superfluid turbulence, Phys. Rev. Lett. 90 (2003) 205301.
[16] M. Tsubota, C.F. Barenghi, T. Araki, A. Mitani, Instability of vortex array and transitions to turbulence in rotating helium II, Phys. Rev. B 69 (2004) 134515.
[17] D. Kivotides, J.C. Vassilicos, D.C. Samuels, C.F. Barenghi, Kelvin waves cascade in superfluid turbulence, Phys. Rev. Lett. 86 (2001) 3080.
[18] D. Kivotides, C.F. Barenghi, D.C. Samuels, Fractal dimension of superfluid turbulence, Phys. Rev. Lett. 87 (2001) 155301.
[19] C.F. Barenghi, D.C. Samuels, Evaporation of a packet of quantized vorticity, Phys. Rev. Lett. 89 (2002) 155302.
[20] L. Kondaurova, S.K. Niemirowskii, Full Biot–Savart numerical simulation of vortices in superfluid He II, J. Low Temp. Phys. 138 (2005) 555.
[21] T. Lipniacki, Evolution of line-length density and anisotropy of quantum tangle, Phys. Rev. B 64 (2001) 214516.
[22] C.F. Barenghi, D.C. Samuels, G.H. Bauer, R.J. Donnelly, Superfluid vortex lines in a model of turbulent flow, Phys. Fluids 9 (1997) 2631.
[23] O.C. Idowu, D. Kivotides, C.F. Barenghi, D.C. Samuels, Equation for self-consistent superfluid vortex line dynamics, J. Low Temp. Phys. 120 (2000) 269.
[24] R.J. Donnelly, Liquid and gaseous helium as test fluids, in: R.J. Donnelly (Ed.), High Reynolds Number Flows Using Liquid and Gaseous Helium, Eugene, Springer-Verlag, New York, 1991.
[25] K.W. Schwarz, J.R. Rozen, Transient behavior of superfluid turbulence in a large channel, Phys. Rev. B 44 (1991) 7563.
[26] T. Lipniacki, Evolution of quantum vortices following reconnection, Eur. J. Mech. B Fluids 19 (2000) 361.
[27] T. Lipniacki, Shape-preserving solutions for quantum vortex motion under localized induction approximation, Phys. Fluids 15 (2003) 1381.
[28] T. Lipniacki, On quantum turbulence in superfluid ^{4}He, Arch. Mech. 53 (2001) 23.
[29] W.F. Vinen, Mutual friction in heat current in liquid helium II, III. Theory of the mutual friction, Proc. Roy. Soc. London Ser. A 242 (1957) 493.
[30] C.F. Barenghi, Turbulent dissipation near absolute zero, Eur. J. Mech. B Fluids 23 (2004) 415.
[31] C.F. Barenghi, R.J. Donnelly, W.F. Vinen, Quantized Vortex Dynamics and Superfluid Turbulence, Springer-Verlag, Berlin, 2001.
[32] M.R. Smith, R.J. Donnelly, N. Goldenfeld, W.F. Vinen, Decay of vorticity in homogeneous turbulence, Phys. Rev. Lett. 71 (1993) 2583.
[33] W.F. Vinen, Classical character of turbulence in a quantum liquid, Phys. Rev. B 61 (2000) 1410.
[34] W.F. Vinen, J.J. Niemela, Quantum turbulence, J. Low Temp. Phys. 128 (2002) 167.
[35] Z. Peradzynski, W. Fiszdon, S. Filipkowski, Spin-up of He II in a cylindrical vessel of finite height, Eur. J. Mech. B Fluids 9 (1990) 259.
[36] T. Lipniacki, Can the system of discrete vortices imitate boundary layer, Arch. Mech. 49 (1997) 103.
[37] C.E. Swanson, C.F. Barenghi, R.J. Donnelly, Rotation of a tangle of quantized vortex lines in He II, Phys. Rev. Lett. 50 (1983) 190.

[38] D. Jou, M.S. Mongiovi, Phenomenological description of counterflow superfluid turbulence in rotating containers, Phys. Rev. B 69 (2004) 094513 and M.S. Mongiovi private communication.
[39] W.I. Glaberson, W.W. Johnson, Ostermeir, Instability of a vortex array in He II, Phys. Rev. Lett. 33 (1974) 1197.
[40] M.S. Mongiovi, D. Jou, Superfluid turbulence in rotating containers: phenomenological description of the influence of the wall, Phys. Rev. B 72 (2005) 104515.
[41] T. Lipniacki, Dynamics of superfluid Helium – Limits of the Vinen model, Arch. Mech. 49 (1997) 615.
[42] D.C. Samuels, Velocity matching and Poiseuille pipe flow of superfluid helium, Phys. Rev. B 46 (1992) 11714.
[43] C.F. Barenghi, S. Hulton, D.C. Samuels, Polarization of superfluid turbulence, Phys. Rev. Lett. 89 (2002) 275301.